Receptor stoichiometry predicts artery-typical vulnerability to altered Notch signaling during smooth muscle differentiation.

Sami Sanlidag[1,2,3], Noora Virtanen[1,2,3,a], Hesam Hoursan[4,5,a], Tommaso Ristori[4,5], Marika Sjöqvist[1,2], Sandra Loerakker[4,5], Cecilia Sahlgren[1,2,3,4,5,6]

[1]Faculty of Science and Engineering, Cell Biology, Åbo Akademi University, Tykistökatu 6, FI-20520, Turku, Finland
[2]Turku Bioscience, Åbo Akademi University and University of Turku, Tykistökatu 6, FI-20520, Turku, Finland
[3]InFLAMES Research Flagship Center, Åbo Akademi University and University of Turku, Turku, Finland
[4]Department of Biomedical Engineering, Eindhoven University of Technology, PO Box 513, 5600 MB, Eindhoven, the Netherlands
[5]Institute for Complex Molecular Systems (ICMS), Eindhoven University of Technology, Ceres, Building Number 7, De Zaale, 5612 AJ, Eindhoven, the Netherlands
[a] These authors contributed equally.
[6]Lead contact (Cecilia.sahlgren@abo.fi).

Keywords:

Notch signaling, vascular smooth muscle, artery development, arterial disease

ABSTRACT

The development and maintenance of arterial smooth muscle cells (SMCs) rely on Jagged1-Notch2/Notch3 signaling. While Notch2 and Notch3 are thought to function redundantly during SMC development, clinical and experimental evidence suggests artery-specific importance for the two receptors. Combining *in vitro*, *in vivo,* and *in silico* models, we report that the canonical Notch signaling during SMC differentiation is largely driven by Notch2. While Notch2 and Notch3 co-regulate a large group of genes in SMCs upon Jagged1 interaction, Notch3 is a less potent inducer of Notch signaling than Notch2 and requires higher doses to potentiate a meaningful transcriptional response due to its weak interaction with RBPJκ. Consequently, Notch2 depletion abolishes Notch signaling in the SMCs of the large elastic arteries. However, high Jagged1 and Notch3 expression in smaller arteries like those in the brain can compensate for Notch2 loss. This work refines our mechanistic understanding of Notch signaling in the SMCs and offers region-specific insights into the Notch-related arterial diseases.

INTRODUCTION

Vascular smooth muscle cells (SMCs) form a multilayered wall around the endothelium in larger caliber blood vessels, such as arteries, arterioles, and veins, ensuring vascular integrity and function. The dysregulation of SMCs is linked to severe vascular complications and constitutes high clinical significance. However, our understanding of the mechanisms regulating the SMC differentiation in different arteries is incomplete, hindering the development of appropriate therapies for SMC-related pathologies.

During development, vascular SMCs proliferate and produce the extracellular matrix around the endothelium(1, 2), followed by SMC maturation. The mature SMCs are contractile and contribute to the vascular tone. In case of alterations in the vascular environment, they can switch between varying phenotypes to partake in vascular adaptation through several mechanisms, including proliferation(3). Notch signaling, a contact-dependent cell-cell signaling pathway, is a master regulator of SMC development and homeostasis(4). In mammals, Notch signaling comprises four transmembrane Notch receptors (Notch1, 2, 3, and 4) and five ligands (Jagged1 and 2; and Delta-like 1,3, and 4). When a ligand pulls on a Notch receptor, the receptor becomes poised for two consequent cleavages mediated by ADAM (S2 cleavage) and γ-secretase (S3 cleavage), respectively. This liberates the active Notch intracellular domain (NICD) that can translocate to the nucleus and drive transcription through its co-factors, such as RBPJκ(5, 6). Generally, the receptor-ligand interactions between two juxtaposed cells (trans-interactions) activate the receptor, while those on the same cell (cis-interactions) are considered inhibitory(7). Notch signaling drives the specification and expansion of SMCs by regulating platelet-derived growth factor receptor β (Pdgfrβ) levels(8, 9) and controls their maturation by regulating contractile gene expression and quiescence(10, 11). Furthermore, it propagates around the endothelium through a mechanism called lateral induction, where the Notch activity driven by the endothelial Jagged1 leads to the expression of the SMC-intrinsic Jagged1, which activates Notch in the surrounding cells, thereby contributing to the vascular wall assembly(12–14).

Vascular SMCs mainly express receptors Notch2 and Notch3 and ligand Jagged1. Dysregulation of these molecules can cause vascular complications affecting different vessels in the arterial tree. Alagille syndrome (ALGS) is a congenital disorder attributed to mutations in Jagged1 and, less frequently, Notch2(15). It manifests with multisystem complications all around the body, including intracranial hemorrhages, aneurysms, and outflow tract defects (16–18). Notch3 is linked to perivascular complications in pulmonary hypertension, such as hypermuscularization and stenosis(19). Cerebral autosomal dominant arteriopathy with subcortical infarcts and leukoencephalopathy (CADASIL) is caused by mutations in Notch3 and manifests with dementia and smooth muscle loss in smaller caliber arteries and arterioles(20, 21). Similarly, transgenic animals lacking these proteins show perivascular pathology. Mice with endothelial cell-specific knockout of Jagged1 are deficient in SMCs and die early during embryonic development(22). Notch2 hypomorphic (Notch2$^{del1/del1}$) mice show abnormalities, such as attenuated contractile marker expression and structural defects in the larger elastic pulmonary arteries and aorta, as well as significantly increased rates of patent ductus arteriosus (failure in the closure of the ductus arteriosus) and mortality shortly after birth(10, 23, 24). Notch3 knockout does not cause a lethal periarterial phenotype in the developing mouse, apart from mild reduction in the late contractile

markers(25, 26) and later defects in the myogenic tone and SMC distribution in small vessels, such as those in the tail and the brain (27–29). However, the combination of Notch2 hypomorphism and Notch3 knockout is embryonically lethal due to severe perivascular defects, implying overlapping functions between the two receptors (10). There is also evidence supporting opposing roles for Notch2 and Notch3 in vascular SMC growth and homeostasis. Notch3 promotes proliferation and survival in concert with the ERK signaling(30) *in vitro,* and its elevated activity is linked to the overgrowth of SMCs during pulmonary hypertension(19) and in the aorta of elastin-null mice(31). Meanwhile, Notch2 promotes cell cycle arrest by p27 stabilization(11). Despite these indications, a systematic understanding of how Jagged1 signals through Notch2 and Notch3 to regulate different cellular processes during vascular SMC development has been missing.

In this work, we sought to understand the signaling mechanism involving Jagged1, Notch2, and Notch3 and how they regulate SMC differentiation in different arteries in the body. First, using *in vitro* assays and a whole transcriptome analysis, we found that Notch2 and Notch3 co-regulated transcriptional programs relating to periarterial development following Jagged1 induction in a time-dependent manner. However, the two receptors differed in their ability to potentiate transcription. Notch2 and Notch3 responded similarly to Jagged1 at the protein level, but Notch2 ICD was transcriptionally more robust. Notch3 ICD could reach substantial transcriptional activity only when it was present at high levels. Furthermore, through *in situ* hybridization and single-cell transcriptomic databases, we found that SMCs at different arteries varied highly in Notch3 and Jagged1 expression. By integrating these findings into a computational model of Notch signaling in arteries, we predicted artery-typical vulnerability to altered Notch signaling in the SMCs, where hypoactivity of Notch2 and Jagged1, but not of Notch3, severely affected Notch signaling. However, SMCs of the arteries with high levels of Notch3 and Jagged1 were predicted to be less dependent on Notch2. Contractile gene reporter assays in zebrafish larvae injected with Notch2 and Notch3 morpholinos recapitulated these predictions, showing that Notch3 can compensate for Notch2 depletion in SMCs of the cerebral vessels that express high levels of Notch3. Overall, our work provides clues for how the altered Jagged1-Notch2 and -Notch3 axes can contribute to human periarterial disease onset with local specificity.

RESULTS

Notch2 and Notch3 act as functional analogs during Jagged1-mediated vascular smooth muscle differentiation, but Notch2 is more robust.

To systematically address the functions of Notch2 and Notch3 in the Jagged1-mediated SMC phenotypic regulation, we chose an *in vitro* approach and used immobilized recombinant human Jagged1-Fc dimeric proteins (J1-Fc) to activate Notch signaling in human aortic SMCs, followed by bulk RNA sequencing (Fig. 1A). First, we silenced Notch2 or Notch3 in the SMCs using siRNAs (siN2, siN3). 48h post-transfection, Notch2 and Notch3 protein levels were significantly reduced compared to the cells transfected with the non-targeting control (siC) (Fig. 1B), demonstrating successful silencing of the receptors. We saw a slight reduction in the Notch3 levels with siN2 (Fig. 1B; S1A,K). This was expected since Notch3 is a transcriptional target of Notch2(10). Neither of the siRNAs led to an appreciable change in Notch1 mRNA (Fig. S1A). We then plated the cells on immobilized J1-Fc and harvested them for RNA extraction after 4 and 24 hours to capture an early, more Notch-specific transcriptional response, and a later response relating to the SMC differentiation program, respectively. By setting thresholds of fold change (FC) >2 and false discovery rate (FDR) <0.05, we identified 78 genes at 4h (47 up- and 31 downregulated) and 583 genes at 24h (249 up- and 334 downregulated) differentially regulated by Jagged1 induction in the control cells. The top 10 up- and downregulated genes are annotated in Fig. 1C (See Dataset S1 for a complete list of the DEGs).

At 4h, many putative Notch targets, such as HEY1, HEYL, HES1, NRARP, and JAG1, as well as genes related to perivascular identity (KCNE4(32)), SMC quiescence (CDKN2B(33)), and TGFβ signaling effectors (TGFB3 and SMAD3), were upregulated. Interestingly, the silencing of Notch2 and not of Notch3 led to a dramatic loss of transcriptional response to Jagged1, as evidenced by the overall behavior of the gene cluster across the groups (Fig. 1D; S1D). This pattern was reflected in many of the Notch targets, such as HEY1 and NRARP (Fig. 1F). Only a few genes, such as KCNE4 and TGFB3, seemed to be affected by Notch3 silencing to a similar degree to Notch2 (Fig. S1A) even though these cells express NOTCH3 mRNA approximately twice as much as Notch2 under basal conditions (Fig. S3A).

At 24h, the earlier markers of SMC contractility such as ACTA2, CALD1, and LMOD1, but not the mature SMC markers, such as MYH11 and SMTN (Fig. 1 A), were among the upregulated genes, confirming an intermediate stage of contractile differentiation following the receptor activation by immobilized Jagged1. On the other hand, the transcriptional response was convoluted at this time point, and it was difficult to discern between the Notch2- and Notch3-silenced groups using simple statistical comparison. For easier interpretation, we divided the DEGs at 24h into five Ward clusters (2 up- and 3 downregulated clusters) (Fig. 1D, also see Dataset S1 for the clusters). Both upregulated clusters, *c* and *d*, were enriched for ontology terms related to vascular myogenic processes, while the three downregulated clusters, *a*, *b,* and *e,* were enriched for vascular process-, synaptic signaling-, and cell cycle-related terms, respectively (Fig. S1C).

Notch2 silencing also had a profound impact on all clusters at 24h. This effect was particularly evident in *cluster a* and the majority of *cluster c (See Fig. S1D for cluster behavior),* which were affected little by Notch3 silencing. SNAI2 (Fig. S1B), an important transcription factor for the

recruitment of mural progenitors around the aorta from the sclerotome, was also specifically regulated by Notch2 silencing (*cluster c*) (34). *Cluster a* included genes such as SOST, RGS2, and EDNRB, which mark different zones in the pulmonary-aortic tree(35), and genes linked to adverse aortic remodeling, FERMT1, and BMP2 (See Dataset S1) (36, 37) - posing the question of whether Notch2 might be important for the identity of the SMCs at this location.

Notch3 silencing elicited a consistent (albeit smaller compared to Notch2) reduction in the ligand-induced transcriptional response at 24h. Overall, it seemed that many genes responded strongly to Notch2 already at 4h, while Notch3 only added to this response at 24h. This pattern was reflected in some genes of *cluster c,* including Notch targets NRARP and HEY1; the perivascular marker PDGFRB (Fig. 1F); and the extracellular matrix components, such as COL5A1 (Fig. S1B). The impact of Notch3 was most evident in c*lusters d* and *e,* which responded to the silencing of Notch2 and Notch3 similarly (Fig. 1D; S1D). These clusters were enriched for genes related to the hallmarks of SMC maturation: contractile markers, extracellular matrix deposition (e.g., COL4A1), and cell cycle arrest (e.g., CDKN2B) (Fig. 1G; S1A). Interestingly, the optimal expression of genes related to SMC contractility, such as ACTA2 encoding for α-smooth muscle actin (αSMA), seemed to rely on both receptors (Fig. 1G). Notch3 knockout mice develop αSMA-positive SMCs, and overexpressing any of Notch1, 2, and 3 intracellular domains (ICD) can induce the SMC contractility genes in a serum response factor-dependent manner (SRF) (10, 38, 39). Thus, it is likely that the combined activity of Notch2 and Notch3 efficiently boosts the contractile differentiation. Following this notion, Notch2 and Notch3 silencing both downregulated pro-contractile genes OLFM2(40, 41), SPON2(42), and FOXS1, all of which were among the top 10 DEGs induced by Jagged1 at 24h (Fig. S1E). Especially, the Forkhead box family gene FOXS1 was highly responsive to Jagged1. It was regulated only by Notch2 at 4h, and both by Notch2 and Notch3 at 24h, similar to the putative Notch targets. FOXS1 is a periarterial marker(43, 44) and regulates TGFβ-mediated ACTA2 expression(45). Consistently, ChEA3(46) predicted FOXS1 as one of the top candidates upstream of *cluster d* (Fig. S1F). Thus, we tested TGFβ signaling and FOXS1 as potential factors favoring contractile differentiation downstream of Jagged1-induction. Silencing FOXS1 led to a non-significant but consistent decrease in ACTA2 and CNN1 expression. Meanwhile, SRF silencing abolished their expression altogether (Fig. S1G). Jagged1 induction or DAPT treatment did not affect SMAD2 phosphorylation. Additionally, inhibiting TGFβ receptor signaling did not affect Jagged1-induced αSMA production or collagen I or IV expression (Fig. S1H-J). These findings suggest that Jagged1-Notch2/3 signaling directly promotes pro-contractile genes that act upstream of SRF.

Upregulation of Notch3 by the Jagged1-Notch2 axis contributes to prolonged Notch signaling.

Considering the delayed contribution of Notch3 to the Jagged1-induced transcriptional response, we sought to understand the temporal relationship between Jagged1, Notch2, and Notch3 better. As Notch3 was already shown to be positively regulated by the Notch signaling(10, 47), we attributed its increased influence at 24h to its upregulation. Indeed, NOTCH3 mRNA was upregulated more than 2-fold upon ligand induction, whereas NOTCH2 mRNA seemed unchanged relative to the basal conditions (Fig. S1A). Interestingly, the Jagged1-induced expression of NOTCH3 was nearly lost upon Notch2 silencing. Similarly, the S1-cleaved Notch3

187 products were significantly downregulated with Notch2 silencing after 72 hours of Jagged1
188 induction (Fig. S2A,C), suggesting that the activation of the basal Notch3 was not sufficient to
189 potentiate its own expression and that this process instead relied on Notch2 activity. To confirm
190 this causal relationship, we performed DAPT washout experiments, where we grew SMCs on
191 immobilized J1-Fc in the presence of DAPT overnight and removed the inhibitor the next day to
192 allow Notch signaling activation. This way, we also hoped to eliminate any bias on the receptor
193 cleavage that might arise from trypsinization at the time of cell plating on the ligands. First, we
194 checked the protein abundance using the wild-type cells (Fig. 2A,B) and confirmed that the signal
195 from the S1-cleaved Notch3 products increased by more than 5-fold starting from 24h. The
196 corresponding bands for Notch2 were reduced by nearly 50% compared to the starting conditions,
197 suggesting that Notch2 might be consumed at a faster rate, possibly due to the absence of similar
198 positive feedforward mechanisms for this receptor. Next, we included SMCs with Notch2 or
199 Notch3 silencing in a similar setting (Fig. 2C). The qPCR results recapitulated the same trends,
200 showing that the effect of Notch3 on Notch target gene expression (HEY1 and JAG1) was
201 negligible at 4h, but became more prominent at 24, consistent with the nearly 3-fold increase of
202 the NOTCH3 mRNA following the Jagged1-induction. Again, the upregulation of NOTCH3 was
203 nearly lost with Notch2 silencing, confirming our findings from the RNAseq.

204 To investigate the relevance of the upregulated Notch3, we also checked the abundance of
205 Pdgfrβ, αSMA, the cell-intrinsic Jagged1, as well as the ACTA2, JAG1, and HEY1 mRNAs later
206 at 72h. All molecules, except for Pdgfrβ, showed a negative trend upon Notch3 silencing (Fig. 2C;
207 S2A,C). Contrary to the indications from the RNAseq, Notch3 did not mediate a visible reduction
208 in SMC proliferation in the absence of Notch2 (Fig. S2B), suggesting that the initial levels of
209 Notch3 might not be sufficient to potentiate this effect on its own. We next prepared spheroid
210 cultures using only SMCs or SMCs and endothelial cells (ECs) to eliminate extrinsic J1-Fc ligands
211 and instead enforce the native cell-cell Jagged1-Notch signaling. At 72h, both spheroids showed
212 a similar reduction in the immunostaining of Jagged1 with Notch2 and Notch3 silencing (Fig. S2D
213 and E), supporting that Notch3 contributes to the long-term Notch signaling response. These
214 results together suggest that the initial Notch signaling "push" by the Jagged1-Notch2 axis is
215 necessary for Notch3 expression, which then contributes to the long-term Notch signaling during
216 *in vitro* SMC differentiation (See Fig. 2D for the schematic description of the proposed
217 mechanism).

218 **Elevated levels of Notch3 are required for transcriptionally meaningful canonical Notch3**
219 **signaling due to the weak Notch3-CSL interaction.**

220 Next, we wondered why Notch3 relied on amplified expression to produce a sufficient
221 transcriptional response to Jagged1. NOTCH3 is expressed nearly twice as much as NOTCH2 in
222 SMCs, already at the basal levels, eliminating the possibility that the difference in activity was
223 caused by the initial levels (Fig. S3A). Evidence suggests that the interactions between Jagged1
224 and Notch3 rely on additional molecules in SMCs (48–50). Hence, we asked whether receptor
225 availability to J1-Fc could contribute to the weaker signaling from the Jagged1-Notch3 axis. To
226 test this, we used a saturating concentration (10nM) of pre-labeled soluble J1-Fc to stain live
227 SMCs (Fig. 3A). Confocal imaging following the fixation of the stained SMCs showed that
228 silencing of Notch2 and Notch3 caused a visible difference in the fluorescent puncta (Fig. 3B).

229 We repeated the live staining protocol and measured the fluorescence signal using flow cytometry.
230 Again, silencing either receptor caused a comparable decrease in the fluorescence signal (Fig.
231 3C,D). We observed a marginally larger, albeit statistically insignificant, decrease in the mean
232 fluorescence intensity of the Notch2-silenced cells. We attributed this difference to the slight
233 reduction of Notch3 observed with the Notch2 siRNA. Thus, we concluded that the interaction of
234 J1-Fc with Notch2 and Notch3 was comparable. We also investigated receptor processing
235 triggered by the immobilized J1-Fc at 4, 24, and 72 hours post-DAPT washout due to the evidence
236 that the Notch paralogs vary in sensitivity to cleavage (51–54). We did not find meaningful
237 differences between Notch2 and Notch3 processing, measured by the ratio of the NEXT to the
238 total signal from the NEXT and the NTM bands (Fig. 3E,F). These results together suggested that
239 the large difference in the transcriptional activity of the two receptors could not be explained by
240 J1-Fc binding preference or the differential regulation of receptor processing. We next asked
241 whether the intracellular domains of the two receptors elicited different transcriptional activity. We
242 tested this by expressing increased concentrations of NICD2 and NICD3 constructs bearing Flag
243 tags, together with a 12xCSL-Luciferase reporter and β-galactosidase in HEK 293T cells (Fig.
244 3G,H). NICD2 mediated dramatically higher reporter activity, reaching far beyond the dynamic
245 range of NICD3 even at very low concentrations. To test the interaction between the NICD
246 paralogs and RBPJκ, we co-expressed 6xHis-tagged RBPJκ and each of the three NICD paralogs
247 (NICD 1, 2, and 3) in HEK 293T cells and performed co-immunoprecipitation using beads bearing
248 α-Flag antibody. Western blot and densitometry analyses showed that NICD1 and NICD2
249 interacted more strongly than NICD3 with RBPJκ (Fig. 3I,J).

250 Next, we used computational modeling to ask if the difference in transcriptional activity mediated
251 by Jagged1-Notch2 and Jagged1-Notch3 signaling in SMCs can be explained with the NICDs
252 transcriptional activity. The model, extended from previous versions (13, 14) to include both
253 Notch2 and Notch3 signaling (Fig. S3B,C), could successfully replicate the qPCR data from Fig.
254 2G (the data at 24h), but only when assuming that NICD2 had a much higher potential to drive
255 JAG1 and NOTCH3 expression than NICD3. Based on the optimization, the algorithm predicted
256 that NICD2 would exert a significantly larger influence, more than 2-fold greater, on the production
257 rates of Notch3 and Jagged1 compared to NICD3 (Fig. S3D-F). Our lab has previously shown
258 that the RAM domain of NICD1 has a much lower dissociation constant (K_d=0.022 μM) than
259 NICD3 (K_d=0.187 μM) for RBPJκ, implying higher affinity between NICD1 and RBPJκ(55). NICD1
260 and NICD2 are structurally similar and have been shown to be functionally interchangeable during
261 murine development and carcinogenesis(51, 56). Thus, these results suggest that the weak
262 transcriptional consequence of the Jagged1-Notch3 axis is caused by the low potency of the
263 Notch3 ICD to drive RBPJκ-mediated transcription, and that higher levels of Notch3 are needed
264 for meaningful Notch signaling output during SMC differentiation.

265 **Levels of Notch3 predict artery-typical vulnerability to altered Jagged1-Notch2/Notch3**
266 **signaling in the SMCs.**

267 Vascular SMCs show remarkable heterogeneity in their transcriptional profile, which contributes
268 to region-specific vulnerabilities to perivascular disease (57–59). Likewise, Notch3 expression in
269 the outflow tract has been suggested to depend on the embryonic lineage, where the SMCs of
270 the neural crest origin show higher Notch3 expression than those derived from the sclerotome

and the second heart field(25). Therefore, we wondered whether possible regional differences in the expression of Notch components and their differential ability to induce canonical Notch signaling could help explain receptor-specific effects in perivascular disease onset. We started by mining the expression of Notch signaling components in the arterial cells from multiple locations using previously published single-cell RNAseq data from adult mice (35, 57, 60) (Fig. 4A; S3I,H). Notch2 was expressed at relatively low levels in all arteries and showed little variation. Surprisingly, Notch3 expression varied vastly among the SMCs of different arteries. It was expressed highly in smaller muscular arteries, such as the arteries in the heart, the brain, and the colon. Meanwhile, the aorta, the proximal and the distal regions combined, had strikingly little Notch3 in comparison.

Next, we aimed to see how expression of the two receptors could affect the Notch signaling output in the arterial wall. Using the optimized parameters relating to the Jagged1-Notch2/3 signaling from our simulations (Fig. S3F - Also see Table S2 in Supporting Methods), we extended the computational model of Notch signaling in the arteries that was previously adapted and tested by our lab (13, 61–63) (Fig. 4B). The new model takes Notch2 and Notch3 dynamics during Jagged1-mediated lateral induction into account and calculates a "Notch multiplier" (Notch multiplier=1 indicates basal Notch activity) as a measure of the Notch signaling activity in a simulated arterial wall. We then adjusted the basal Jagged1, Notch2, and Notch3 production rates in SMCs ($N_2^{pr}, N_3^{pr}, J^{pr}$) in a range between 0 and 3000 h^{-1} to predict the Notch multiplier in different Notch2/Notch3 stoichiometries (Fig. 4E). The model was highly sensitive to Jagged1 and Notch2 manipulations, as the Notch multiplier rapidly changed with respect to J^{pr} and N_2^{pr}. This is also consistent with the previously reported *in vivo* findings, where combined heterozygous Jag1$^{\Delta DSL}$ and Notch2^{del1} mutations in mice closely recapitulate the ALGS phenotype (64). Meanwhile, increasing N_3^{pr} by itself had little impact on the Notch multiplier and its contribution was merely additive to that of N_2^{pr}, corroborating our *in vitro* data.

To put the Notch multiplier in a physiological perspective, we chose Notch stoichiometries resembling those in different arterial SMCs. Considering the low expression of Notch2 and the relatively higher Notch3 expression in all arterial SMCs, we assigned simple Notch2^{Low}/Notch3^{Low} (N_2^{pr}= 500 h^{-1}, N_3^{pr} = 1000 h^{-1}) and Notch2^{Low}/Notch3^{High} stoichiometries (N_2^{pr}= 500 h^{-1}, N_3^{pr} = 3000 h^{-1}) for aortic and pulmonary SMCs, respectively. We set the minimum J^{pr} to 1000 h^{-1}, since otherwise, the Notch multiplier was not meaningful with the chosen ranges of N_2^{pr} and N_3^{pr}. For the muscular arterial SMCs (heart, colon, and brain arterial SMCs), we used the same Notch2^{Low}/Notch3^{High} stoichiometry but set J^{pr} to 3000 h^{-1} in line with the higher Jag1 expression seen in these cells. This way, we could fit the numbers representative of different arterial SMCs within the dynamic range of our simulations (Fig. 4D). This approach yielded Notch multipliers resembling the trend of Nrarp expression, a proxy for Notch activity, across different arterial SMCs (Fig. S3H). Furthermore, setting J^{pr} to 0 with the aortic receptor parameters reduced the Notch multiplier from 2.24 to nearly 1 (Fig. S3G), resulting in a similar negative 2-fold change that was seen with Notch target expression in the mouse aortic smooth muscle tissue upon Jagged1 knockout (65).

Further, we explored loss-of-function scenarios for Notch2 or Notch3 by setting the production rates of either to 0. The model predicted that Notch2 knockout, but not Notch3 knockout, reduces the Notch multiplier in all arterial conditions significantly (Fig. 4D). Setting N_2^{pr} to 0 resulted in an approximately 2-fold decrease in the Notch multiplier in the aortic SMCs (2.24 to 1.12), leading to almost a complete loss of the Notch activity. Although the pulmonary SMCs expressed three times as much Notch3, the decrease in the Notch multiplier with Notch2 knockout was comparable with the aortic SMCs (2.02 to 1.33), consistent with the importance of Notch2 in the outflow tract. The Notch multiplier in the muscular arterial SMCs, which express three times as much Notch3 and Jag1 as their aortic counterparts, was reduced from 4.61 to 1.73 with Notch2 knockout. However, we observe that 1.73 is reasonably close to the Notch multiplier that the model predicted for the aorta and the pulmonary arteries (approximately 2) in the basal conditions. Therefore, one can argue that this level of Notch activity might be sufficient during SMC development. These results suggest that elevated expression of Notch3 can induce sufficient canonical activity, provided high basal Jagged1 expression in the SMCs. Since periarterial lateral induction is triggered by the EC-bound ligands (12, 66), we checked the ligand expression in ECs from the same organ datasets. The ECs of the muscular arteries did not show elevated Jag1, unlike the SMCs (Fig. S3I). However, ECs express high levels of Dll4, which has been shown to contribute to the signaling between the coronary endothelium and the developing SMCs (67). Thus, Dll4 and Jagged1 together might induce sufficient Notch signal in the first layer of SMCs to kickstart lateral induction in the developing media. Supporting this notion, mice with SMC-specific knockout of Jagged1 develop an SMC layer adjacent to the endothelium in the descending aorta, but this layer is much thinner compared to the wildtype, highlighting the importance of Jagged1 of the SMC-origin (68).

Overall, our model predicts that Notch3 depletion has a negligible impact on the periarterial Notch signaling in the presence of Notch2, and that Notch2 depletion is highly detrimental, especially for the aortic-pulmonary tree. On the other hand, it predicts that expression of Notch3, particularly in smaller muscular arteries where it is expressed highly, can partially compensate for Notch2 depletion, but the compensatory effect of Notch3 is dependent on the complementary expression of Jagged1, highlighting the importance of this ligand and its expression level during periarterial development.

Developing SMCs at the cerebral base can compensate Notch2 depletion in the zebrafish larvae.

We tested if we could capture the artery-typical outcomes for impaired Notch2 and Notch3 signaling predicted by our model, in an *in vivo* developmental setting. For this purpose, we chose zebrafish larvae, an established model for vascular development (69). Zebrafish larvae with Notch2 and Notch3 deletion were shown to have a reduced number of pdgfrb^{High} early mural cells in the dorsal aorta (DA), and the cerebral base arteries, BCA (basal communicating artery) and PCS (posterior communicating segment), respectively (9). Thus, we started by assessing the Notch receptor expression in the developing zebrafish perivascular cells in these locations (Fig. 5A). There are no reliable antibodies for the zebrafish Notch orthologs; thus, we performed *in situ* Hybridization Chain Reaction (HCR) in 3dpf (3 days post-fertilization) larvae expressing a pdgfrb reporter using probes against notch2 and notch3. We could not reliably quantify the total intensity or the number of mRNA puncta per cell, due to the difficulty of segmenting the pdgfrb^{High} cells and

353 the irregular signal from notch3. However, notch3 stained more consistently and was localized in
354 broader pdgfrb+ areas in the cerebral base, while the staining was sparser in the dorsal aorta. On
355 The signal from notch2 looked similar in both regions and appeared as sparse puncta (Fig. 5B,C).

356 For a more quantitative approach, we turned to a single-cell RNAseq dataset from Zebrahub (70).
357 Here, we chose to look at the mesoderm dataset, since mural progenitors at the cerebral base
358 and the dorsal aorta mainly derive from this lineage (71). We extracted the cell cluster, compiling
359 all SMCs under the annotation “visceral muscle”. We then created UMAP projections using the
360 Seurat package (72) (Fig. 5D) and identified the vascular SMC clusters by sorting out the cells
361 expressing non-vascular SMC markers desmb, nkx2.3, rem1, and tlx1 (Fig. S4A). Among the
362 remaining, the clusters #1, #3 and #5 were positive for the SMC markers acta2, tagln, and myh11a
363 (Fig. S4). Out of these clusters, cluster #1 expressed dramatically higher levels of notch3
364 compared to the others (Figure 5F,G). These cells are enriched for the head SMC marker foxc1
365 (73) and pericyte-associated signatures (pdgfrb, zeb2a, rasl12, and cd248a) (Fig. S4A) consistent
366 with the more pericyte-like properties of the SMCs in the smaller cerebral (74) and coronary
367 arteries (26), and cluster closely with pharyngeal arch and periocular mesenchyme cells in the
368 original dataset (Fig. S4B,C). Moreover, unlike the other SMC clusters, these cells were largely
369 negative for spatially restricted homeobox genes (e.g., hoxc1a and hoxc8a), somite/trunk
370 signatures (eno3 and fbp2), and fibroblast-like markers (pdgfra and tgfbi) (Fig. 5E; S4A) (75),
371 suggesting that they are from vessels anterior to hindbrain. They also showed higher levels of
372 jag1b and a notch2^{Low}/notch3^{High} stoichiometry (Fig. 5G), recapitulating the same expression
373 pattern as the murine brain SMCs.

374 Finally, to test whether elevated notch3 could drive the differentiation of these cells without the
375 need for notch2, we injected embryos bearing tagln and kdrl reporters with notch2 or notch3
376 morpholinos. Light sheet microscopy at 102 hpf (hours post-fertilization) revealed that the notch2
377 morphants had a significantly decreased number of tagln+ objects around their dorsal aorta,
378 whereas the notch3 morphants were indistinguishable from the control fish, supporting the
379 negligible contribution of notch3 to SMC differentiation in this location (Fig. 5H,I). At BCA and
380 PCS, the number of could not detect any differences between the notch2 morphants and the
381 control. However, consistent with the loss of the pdgfrb^{High} cells in this location with notch3
382 knockout (9), the notch3 morphants showed a negative trend in the number of tagln+ objects (Fig.
383 5H,I). Overall, these results suggest that developing zebrafish SMCs with elevated Notch3
384 expression could tolerate Notch2 depletion during SMC differentiation, corroborating our
385 simulations.

386 **DISCUSSION**

387 Notch signaling is integral in perivascular cell specification, maturation, and homeostasis. As a
388 result, its dysregulation is linked to congenital and acquired diseases with catastrophic
389 consequences for the vasculature. Here we studied the signaling mechanism governing Jagged1
390 and the receptors Notch2 and Notch3, and how it regulates arterial SMC development. Our
391 findings support a causal role of Notch2 for Notch3 (10). We show that when induced with
392 Jagged1, Notch2 and Notch3 both regulate genes related to vascular SMC specification,
393 maturation, and quiescence, albeit with lower transcriptional activity by Notch3. This supports the
394 previous notion that the two receptors could essentially be mutually compensatory during SMC

395 development (9, 10). We cannot state that Notch2 and Notch3 specifically regulate different genes
396 without NICD-DNA interaction assays, such as ChIPSeq, especially given the temporal
397 relationship between Notch2 and Notch3. Thus, we do not exclude the possibility that they might
398 otherwise have specific targets that are not directly related to SMC differentiation, considering the
399 genes associated with the pulmonary-aortic tree regulated by Notch2 in our RNAseq data. As for
400 Notch3, we could not detect any specific signatures among the Jagged1-induced genes that
401 would suggest a pro-growth/survival function as previously suggested (30, 76). Therefore, the
402 canonical Jagged1-Notch3 signaling does not directly explain pathological SMC growth related to
403 increased Notch3 activity or decreased SMC survival upon Notch3 loss. Instead, Notch3 might
404 have paradoxical functions due to non-canonical mechanisms independent of Jagged1. Indeed,
405 it was shown to go through ligand-independent cleavage to promote cell growth in basal breast
406 cancer (77) and signal non-canonically by interacting with β-catenin to promote cell survival in
407 lung cancer (78). Considering that Notch3 itself is upregulated as a result of Jagged1-Notch
408 signaling, in a perivascular context, one must carefully consider whether a particular effect is
409 linked directly to the Jagged1-Notch3 axis or the enhanced cell-autonomous functions of Notch3
410 due to its increased abundance.

411 We show that the Jagged1-Notch3 axis is weaker in inducing a transcriptional response compared
412 to Notch2 and relies on the high abundance of both Jagged1 and Notch3. This has the following
413 implications for the Notch-related vascular disease context. First, the low canonical activity of
414 Notch3 would imply a heavier burden on the Jagged1-Notch2 axis during smooth muscle cell
415 development than previously thought, especially for those in the aorta, where Notch3 is expressed
416 in lower quantities compared to the smaller arteries. This is consistent with the severe
417 deformations observed in the outflow tract of mice with Notch2 and/or Jagged1 depletion, such
418 as patent ductus arteriosus (24) and aortic narrowing (23). Similarly, ALGS patients frequently
419 present with narrowing defects in the outflow tract, such as pulmonary stenosis and aortic
420 coarctation (16, 18). It is worth mentioning that, unlike a severe Notch2 depletion scenario we
421 explored in our experiments, Notch2 mutations reported in the ALGS patients are often
422 heterozygous missense mutations that would lead to a moderate reduction in the receptor activity.
423 Consistently, while total Notch2 knockout alone is embryonically lethal in mice on E10.5(79), the
424 hypomorphic Notch2$^{del1/del1}$ mutation can be partially rescued by Notch3 even in the developing
425 mouse aorta (10). This might help explain why Notch2-type ALGS is not as strongly associated
426 with vascular defects as are the Jagged1-type cases. Other evidence suggests that the induced
427 knockout of Notch2 in adult mice does not affect the neointimal area following carotid injury (80)
428 or diet-induced atherosclerotic plaque formation (81). However, Notch2 activity might be more
429 integral during the development of SMCs than in their homeostasis or injury response, since in
430 the latter case, the perivascular tissue is already established and rich in supporting extracellular
431 matrix that can switch on compensatory mechanisms. Indeed, in the absence of elastin,
432 epigenetic mechanisms boost Jagged1-Notch3 signaling in the aorta (31). Similarly, carotid injury
433 leads to transient expression of Notch1, which contributes to injury response (82).

434 Second, due to the low transcriptional contribution of Notch3, our results indicate that perivascular
435 defects related to the dysregulation of the Jagged1-Notch3 axis (e.g., in CADASIL) might be
436 associated with the sustainment of the differentiated SMC state and homeostasis, rather than
437 early SMC development. Consistently, the late contractile SMC marker Myh11, but not the SMC

precursor emergence, is affected by Notch3 depletion in the mouse heart (26). Additionally, there is growing consensus that the molecular mechanism underlying the poor SMC coverage in CADASIL is the abnormal accumulation of the Notch3 ECD on the cell surface due to the obstruction of its ligand-dependent elimination, pointing at a gain-of-function effect of Notch3 rather than defective canonical Notch3 signaling (83–86). A Jagged1 mutation in mice phenocopying the human ALGS (Jag1^{Ndr}) shows partial loss in its binding capacity to Notch3 ECD(87) and causes poor SMC coverage in the retinal arterioles and the coronary arteries with increased SMC apoptosis (88) similar to CADASIL, asking whether this phenotype links to a defect in the elimination of the Notch3 ECD. Here we show that smaller muscular arteries like those in the brain and the heart express elevated levels of Notch3, which could boost Notch3 ECD accumulation in these locations and contribute to the small vessel specificity of CADASIL. Indeed, mutant Notch3 (R169C) does not cause a change in the expression of Notch3-driven genes in the arteries, but the forced expression of two copies of the mutant in addition to the wild-type Notch3 exacerbates the ECD accumulation and the resulting arteriopathy. Meanwhile, eliminating one copy of the wildtype Notch3 alleviates the phenotype (89), supporting a Notch3 overdose mechanism over a Notch3 hypo-signaling scenario. Additionally, we have previously shown that Notch3 and Jagged1, but not Notch2, are negatively regulated by strain (13, 90). Thus, it is likely that altered hemodynamics, like high blood pressure, has a considerable impact on how Notch3 functions in smaller arteries during disease. Overall, the differences in the canonical activity of Notch2 and Notch3, and the artery-typical variations in their stoichiometry, can partly explain the locally restricted periarterial phenotypes and clinical findings relating to dysregulation of Jagged1, Notch2, and Notch3.

LIMITATIONS OF THE STUDY

This study has several limitations. Most importantly, our findings are based on the mRNA level expression, and thus, we cannot dismiss the possibility that Notch2 and Notch3 are regulated differently at the protein level. Indeed, contrary to our predictions, Notch3 knockout alone causes an almost complete loss of perivascular cells in the cerebral base of zebrafish larvae (9), showing that Notch2 cannot compensate for Notch3 depletion in this location. While we found that all vascular SMC clusters in zebrafish larvae expressed comparable levels of Notch2 based on Zebrahub, in reality, only a small fraction of the cells in the cerebral arteries were found to be positive for Notch2 reporter activity(9). Thus, we acknowledge the need for improved tools to assess different Notch protein levels *in vivo* and say whether some cells might rely solely on Notch3. Additionally, Notch targets respond differently to the temporal abundance of NICD (91) and might be regulated by co-transcriptional factors in addition to RBPJκ (92). Indeed, cerebral-enriched Foxc1 boosts NICD activity in the zebrafish (93). Notch3 might activate contractility-related genes more efficiently than the other putative Notch targets, as implied by our RNAseq data. Thus, we cannot exclude the possibility that the transcriptional influence of Notch3 might be higher than our predictions. Finally, we did not include the possible influence of Notch1 in our model, which was lowly expressed in our cultured cells as well as the scRNAseq datasets we investigated. Notch1 knockdown was shown to not affect periarterial cell emergence in the zebrafish trunk or brain(9). Similarly, heterogeneous Notch1 knockout does not affect SMC markers(94). However, we cannot rule out a possible compensatory effect from Notch1 in the absence of Notch2 or Notch3.

AUTHOR CONTRIBUTIONS

SS, MS, and CS conceptualized the work. SS, NV, HH, and TR designed the experiments. SS, NV, HH, and TR executed the experiments, analyzed the data, and prepared the figures. SS wrote the initial draft. SS, NV, HH, TR, MS, SL, and CS revised and edited the draft. TR, MS, SL, and CS supervised the study. TR, SL, and CS acquired funding for the study.

FUNDING

This project has received funding from the European Research Council (ERC) and the European Union's Horizon 2020 research and innovation program under grant agreement No. 771168 (ForceMorph) and the European Research Council (ERC) grant agreement No. 802967 (MechanoSignaling). The research has also been supported by the Academy of Finland, decision numbers #316882 (SPACE), #330411 (SignalSheets), #336355 (Solutions for Health at Åbo Akademi University), and #337531 (InFLAMES Flagship Programme). We have also received funding from the Swedish Cultural Foundation, the Finnish Cultural Foundation, the Sigrid Juselius Foundation, Åbo Akademi University Foundation's Centers of Excellence in Cellular Mechanostasis (CellMech), Bioelectronic Activation of Cell Functions (BACE), Jane and Aarno Errko Foundation, and the Finnish Society of Sciences and Letters.

ACKNOWLEDGEMENTS

The bulk RNA sequencing and the data analysis were done in the Finnish Functional Genomics Center and the Medical Bioinformatics Center, Turku. All zebrafish work was done in Zebrafish Core Facility in Turku Bioscience. All microscopy experiments were done in the Cellular Imaging Core in Turku Bioscience. We would like to thank previous laboratory trainees Amanda Norren and Ana Ayala Perez for their help with the differentiation assays. We also thank other persons for the following: help with laboratory and administrative work (Alexandra Manea), help with the design of the RBPJκ plasmid (Elenaé Vázquez-Ulloa), guidance and help with flow cytometry assays (Ezgi Özliseli), guidance and help with qPCR assays (Marjaana Parikainen and Kati Kemppainen), guidance and help with light sheet microscopy and image analysis (Markus Peurla and Anna-Mari Haapanen-Saaristo), guidance with zebrafish experiments (Ilkka Paatero), and help with setting up the computational model (Margot Passier).

509 **Methods**

510 Cell culture, Western blotting, RNA extraction, cDNA synthesis and qPCR analysis, microscopy
511 specimen preparation, flow cytometry, re-analysis of the published single-cell RNAseq data, as
512 well as Next Generation Sequencing of bulk transcriptome and data processing, and
513 computational modelling of extrinsic ligand-induced Notch signaling are described in Supporting
514 Methods. All reagents and resources used in this study are detailed in Table S4.

515 Notch trans-activation assays

516 The cells were plated on the immobilized ligands in SmGM®-2 (Lonza Cat. #CC-3182). In all
517 experiments, human IgG_1 Fc (Bio-techne Cat. #110-HG) was used as a negative control. For the
518 DAPT washout experiments, the cells were plated on the ligands in media containing 10μM DAPT
519 ((2S)- N- [(3,5- Difluoro phenyl)acetyl]- L- alanyl- 2- phenyl]glycine 1,1- dimethyl ethyl ester) (Bio-
520 Techne Cat. #2634-10) or DMSO (dimethyl sulfoxide) (Merck Cat. #D2650) as the vector control
521 where appropriate and let recover for 24 hours. The next day, the DAPT was removed by replacing
522 the media with fresh, warm media, and the cells were incubated for the indicated time until use.
523 For the TGFβR inhibition experiments, the cells were plated on the ligands with media containing
524 10μM SB-431542 (MedChemExpress, Cat. #HY-10431), 10μM DAPT, or DMSO and incubated
525 for either 24 hours for qPCR or 72 hours for immunoblotting. The cells were supplied with media
526 containing fresh dilutions of the inhibitors every 24 hours and washed once with cold HEPES-
527 buffered saline (HBS) (Lonza Cat. #CC50-34) before lysis.

528 Ligand binding assays

529 The live Notch staining assay was done as described previously(95) with a few adjustments. 10^4
530 SMCs per cm^2 transfected with siRNAs against Notch2 and Notch3 were plated 24 hours post-
531 transfection and left to incubate for another 24 hours. The next day, the cells were blocked with
532 sterile-filtered SmGM®-2 containing 1% BSA and 10% goat serum (Biowest Cat. #S2000) for 45
533 min at 37°C with 5% CO_2. 50nM Jagged1-Fc was conjugated with anti-human Alexa fluor 488
534 antibodies (Thermo Fisher Scientific Cat. #21091) at a 1:200 dilution in PBS for 1 hour at cold.
535 The ligand dilution was added directly to the blocking media at a 1:5 ratio to achieve a final ligand
536 concentration of 10nM and incubated for 2 hours at 37°C with 5% CO_2. The cells were either used
537 for microscopy following fixation or live for flow cytometry.

538 Notch reporter assays

539 The luciferase assay was done as described previously(55). HEK 293T cells were transfected
540 with 0.1μg 12xCSL-Luciferase (RBPJκ) and 0.1μg β-galactosidase along with increasing
541 concentrations (0-1.8μg) of Flag-tagged Notch2 or Notch3 intracellular domain (NICD2 and
542 NICD3) constructs. Each transfection was completed with 2μg using the plasmid, only bearing
543 Flag. An extra set of cells was prepared in parallel to assess NICD abundance by immunoblotting.
544 The next day, the cells were lysed in passive lysis buffer (Promega Cat. #E1941). The luciferase
545 activity was measured using VivoGlo™ luciferin (Promega Cat. #P1041) and normalized to β-
546 galactosidase activity.

547 Bulk RNAseq

548 Total mRNA was isolated from SMCs treated with J1-Fc as described in Fig. 1A. The bulk RNA
549 sequencing (RNAseq) was performed in the Finnish Cultural Genomics Center, University of
550 Turku. Processing of the sequencing data analysis was done in the Medical Bioinformatics Center,
551 University of Turku (See detailed pipeline in the SI Methods). Differentially expressed genes
552 (DEGs) upon J1-Fc treatment in the control siRNA-treated samples were used for further analysis
553 for each time point separately. For biological interpretation, z-scores for the DEGs were calculated
554 based on log_2(1+CPM) across all groups from each time point separately. The genes were then
555 clustered using Ward´s method and used to build a heatmap using the pheatmap package
556 (v.1.0.12). Gene ontology analysis for biological processes on each cluster was performed with
557 the clusterprofiler package(v.4.14.4).

558 Immunoprecipitation

559 HEK 293T cells expressing Flag-NICD and 6xHis-RBPJκ were lysed in RIPA buffer (50 mM Tris-
560 HCl pH = 8.0, 1% Triton X-100, 1% sodium deoxycholate acid, 0.1% SDS, 1 mM Na4VO3, 50 mM
561 NaCl, 10 mM NaF, and 1 mM EDTA) containing 1x cOmplete™ protease inhibitors (Roche, Cat.
562 #05892970001) on ice for 10 min. The lysates were scraped into 1.5 ml Eppendorf tubes and
563 centrifuged for 15 min at 14,000 RCF, 4°C. A total of 1.5 mg protein was immunoprecipitated with
564 40µl of anti-Flag affinity agarose beads (Merck, Cat. #A2220) on rotation for 1 hour at 4°C. The
565 beads were washed with the lysis buffer three times and boiled in 3x Laemmli buffer for 10 minutes
566 at 95°C.

567 Zebrafish lines and reporter assays

568 All zebrafish work was carried out in the Zebrafish Core Facility at Turku Bioscience Center under
569 license ESAVI/31414/2020 and ESAVI/44584/2023 granted by the Regional Administration Office
570 of Southern Finland. The offspring of transgenic zebrafish heterozygous for tagln (tagln:GFP) or
571 kdrl (kdrl:mcherry) were injected with 10ng control, Notch2, or Notch3 morpholinos (Gene Tools
572 Store) before the 8-cell stage. Embryos were kept in E3 media (5 mM NaCl, 0.17 mM KCl, 0.33
573 mM $CaCl_2$, 0.33 mM $MgSO_4$) supplemented with 30 mg/ml of 1-phenyl 2-thiourea (PTU) (Merck,
574 Cat. #P7629) at 28.5°C. At 4 dpf, the larvae positive for both reporters were mounted dorsally in
575 2% agarose molds, immobilized with 1% agarose, and imaged in the same media containing 160
576 mg/ml tricaine (Merck, Cat. #E10521) using MSquared Aurora light sheet microscope with 0.4 µm
577 slice thickness. The stacks were stitched using the Zeiss Arivis Vision 4D software (v.3.5.) and
578 analyzed using the Oxford Instruments Imaris image analysis software (v.10.2.0). Briefly, the
579 endothelium marked with kdrl and the tagln+ objects were surface-rendered following pseudo-flat
580 field correction for uneven illumination. The tagln+ objects that were at least in 5µm proximity of
581 the endothelium were considered vascular-associated. In the hind/midbrain region, the objects
582 that were deemed artifacts of the tagln+ tip of the notochord were manually chosen and left out
583 of the analysis. The number of tagln+ objects in the dorsal aorta was normalized to the length of
584 the measured region and presented in arbitrary units.

585 *In situ* hybridization chain reaction (HCR)

586 3 dpf transgenic larvae expressing a pdgfrb reporter (UAS:EGFP, pdgfrb:GAL4FF) were
587 euthanized in E3 media with tricaine at cold for 1h and fixed in 4% PFA overnight at cold. After
588 five washes with PBS, the embryos were dehydrated and permeabilized in methanol at RT four

589 times for 10 min and once for 50 min and rehydrated with four gradually decreasing concentrations
590 of MeOH in PBS with 0.1% Tween 20 (PBST) for 5 min each. The larvae were treated with
591 RNAScope™ Protease Plus (Biotechne, Cat. #322331) for 30 min at RT and quickly washed
592 twice with PBS. The larvae were post-fixed in 4% PFA at RT for 20 min, washed five times with
593 PBS for 5 min each, and used for HCR™ Gold RNA (Molecular Instruments) *in situ* hybridization
594 reaction according to the suppliers' protocol, adapted from Choi et al.(96). The notch2 and the
595 notch3 probes were visualized using x2-546 and x1-647 hairpin pairs, respectively. The fish were
596 mounted ventrally directly on 35 mm glass-bottom confocal dishes (VWR, Cat. #75856) in 1%
597 agarose (w/v) and imaged by taking z-stacks using the 3i CSU-W1 spinning disc confocal
598 microscope with the 25x/0.8 Imm Korr DIC objective with silicone oil (Zeiss). The images were
599 cropped to zoom in on the arterial regions using Fiji ImageJ(97) (v.2.16.0).

600 Statistical analysis

601 All statistical analyses were done using GraphPad Prism (v.10). For single-factor experiments,
602 the normal distribution of the data and the residuals were checked, and one-way ANOVA followed
603 by Tukey´s, Dunnett´s, or Sidak´s post-hoc tests were used. For two-factor experiments, two-way
604 ANOVA followed by Tukey´s, Dunnett´s, or Sidak´s post-hoc tests was used. The data were
605 plotted using GraphPad Prism (v.10) or ggplot2 in R. The p-values smaller than 0.1 were denoted
606 on the plots. The details for the statistical methods and the experimental replicates are given in
607 the Fig. legends.

608 1D Model of Hybrid Arterial Wall

609 To simulate the Notch dynamics in smooth muscle cells (SMCs) within a *hybrid artery* —
610 representing signaling under non-periodic boundary conditions replicating *in vivo* conditions—we
611 adapted an existing computational framework, similar to previous studies(13, 98), we assumed
612 that the first cell in the linear arrangement is an endothelial cell that initiates the signaling cascade
613 through constant emission of Jagged1 (Fig. 4B). SMCs interact with each other as in the previous
614 model, where trans interactions occur between proteins located on the membranes of adjacent
615 cells. Notch and Jagged are both assumed to be evenly distributed across the cell membrane,
616 with half of their total quantity available for binding with each neighboring cell.

617 Considering the significance of Notch in coronary artery dynamics, we selected the geometrical
618 parameters for a coronary artery as the "hybrid artery" to be simulated, assuming an average wall
619 thickness of 0.2 mm(99). The simulated cell line consisted of 20 cells, assuming a cell size of
620 0.01mm, consistent with the arterial thickness. The endothelial cell's constant Jagged1 emission
621 rate was set to 4000 molecules/h, in agreement with previous studies(13, 98).

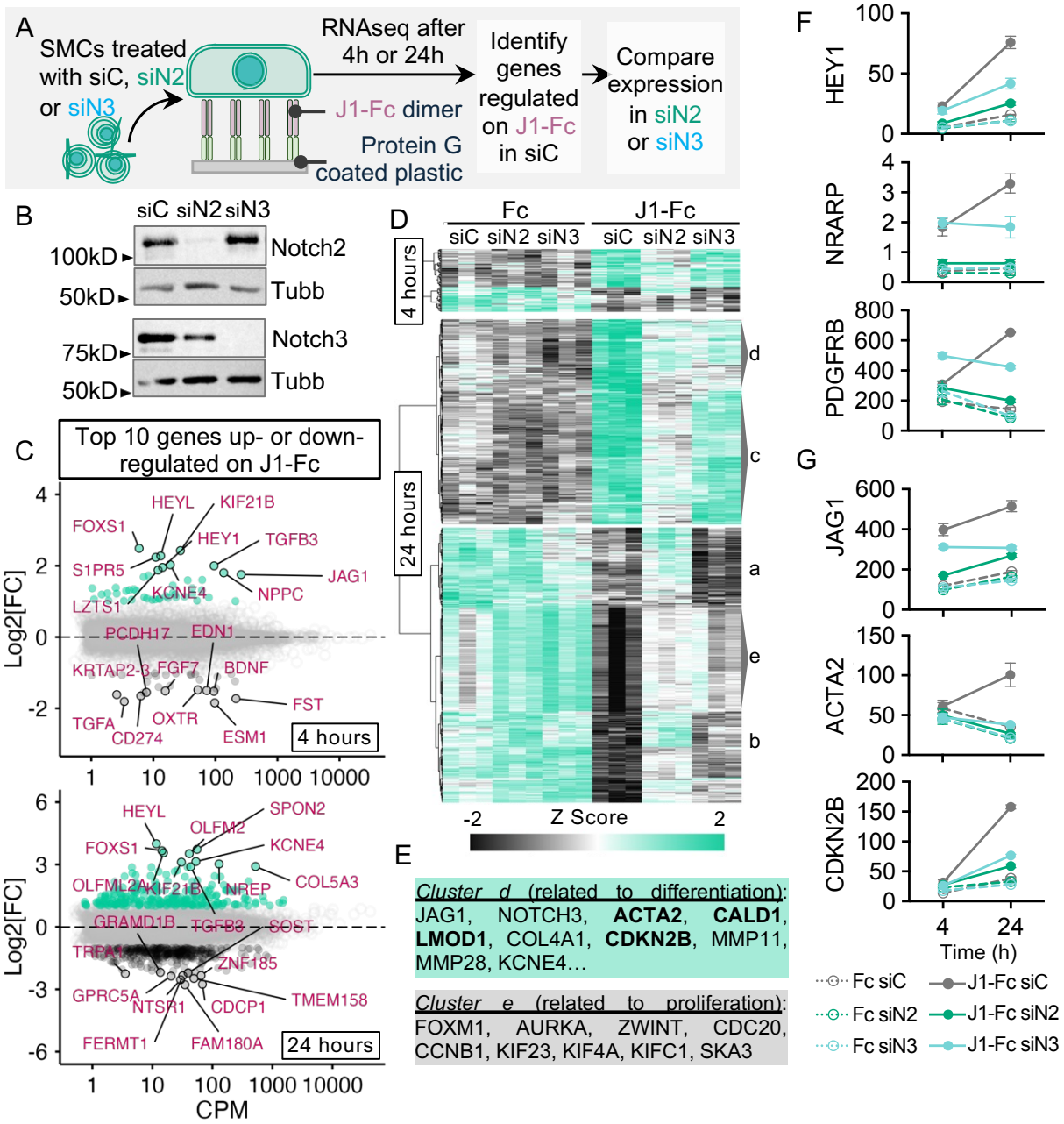

Figure 1. Notch2 and Notch3 act as functional analogs during Jagged1-mediated SMC differentiation, but Notch2 facilitates the early transcriptional response.

(A) Schematic description of the experimental setup and the analysis strategy for the RNAseq experiment.

(B) Notch2 and Notch3 protein levels in SMCs 48h post-transfection with the corresponding siRNAs.

629 (C) Genes significantly regulated in SMCs on immobilized J1-Fc at 4h and 24h (FC>2,
630 FDR>0.05) based on RNAseq. The top 10 up- or downregulated genes are annotated (n=3
631 independent experiments).
632 (D) Heatmaps clustered by Ward´s method showing the z-scores of genes regulated in SMCs
633 on immobilized J1-Fc at 4h and 24h time points across cells treated with control, Notch2, or
634 Notch3 siRNAs (n=3 independent experiments). Gene clusters were considered as follows:
635 Cluster c, upregulated more by Notch2 and less by Notch3; cluster d, upregulated by both
636 Notch2 and Notch3; and Cluster e, downregulated by both Notch2 and Notch3.
637 (E) Representative genes from the clusters on J1-Fc (Cluster d) and genes related to
638 proliferation downregulated on J1-Fc (Cluster e).
639 (F-H) Expression of genes representative of Notch signaling activity, contractile differentiation,
640 and cell cycle arrest (mean±SD).

641

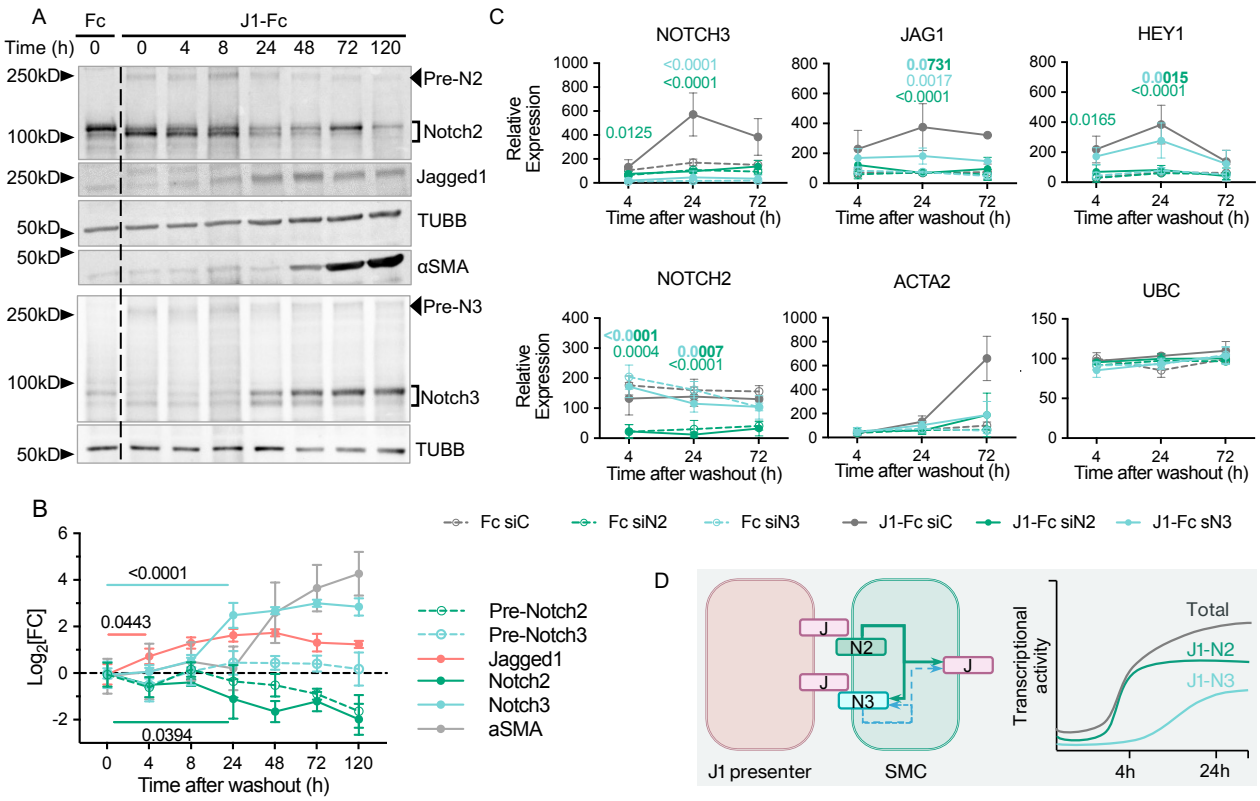

Figure 2. Upregulation of Notch3 by the Jagged1-Notch2 axis contributes to prolonged Notch signaling.
(A, B)SMCs were grown overnight on immobilized J1-Fc in media containing 10μM DAPT. Following DAPT washout the next day, the cells were sampled at the indicated time points. The immunoblot analysis (A) and the quantified signal from the indicated proteins relative to the protein loading are shown (B). Pre-Notch is the full-length precursor before S1-cleavage. The dotted lines represent log2 fold change (mean±SD, n=3 independent experiments, one-way repeated measures ANOVA, and Dunnet´s test for multiple comparisons. Pairwise comparisons with p values smaller than 0.1 are indicated on the plot).
(C) SMCs were transfected with the indicated siRNAs. 24h post-transfection, the cells were plated on immobilized J1-Fc and grown in media containing 10μM DAPT. Following DAPT washout the next day, the cells were sampled at the indicated time points. The dotted lines represent relative expression (mean±SD, n=3 independent experiments (n=2 for 72h). Two-way ANOVA and Tukey´s test for multiple comparisons were performed individually for 4- and 24-hour time points. Pairwise comparisons between J1-Fc-treated samples with p values smaller than 0.1 are indicated on the plots and color-coded for the groups compared.
(D) Schematic description of the working model regarding the temporal relationship between Jagged1, Notch2, and Notch3 and the Notch signaling output over time.

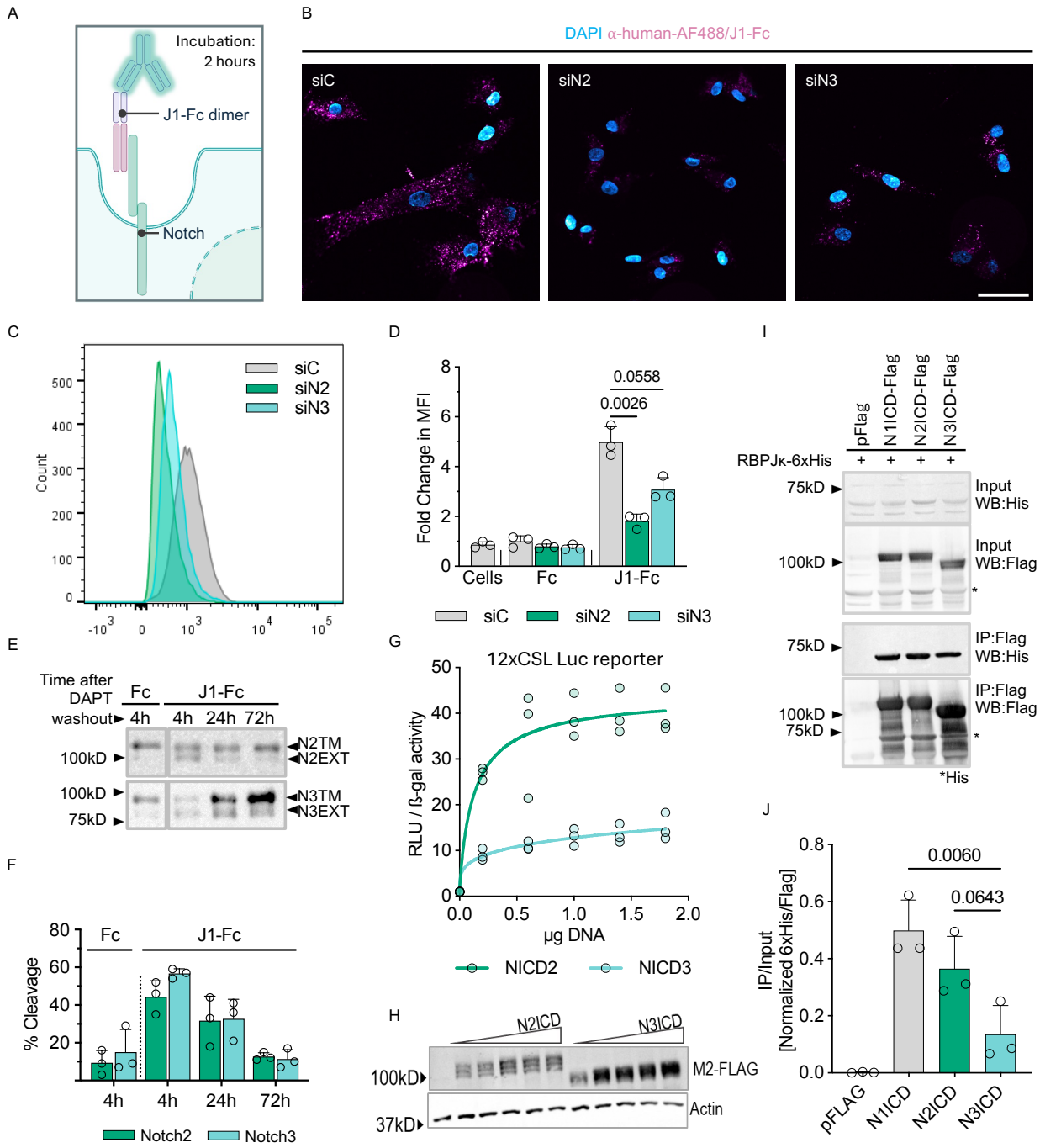

Figure 3. Elevated levels of Notch3 are required for transcriptionally meaningful canonical Notch3 signaling due to the weak Notch3-CSL interaction.

(A-D) SMCs were live-stained with fluorescently labeled J1-Fc 48h post-transfection with the indicated siRNAs to assess ligand-receptor interaction (A). Confocal slices (B) of formalin-fixed SMCs (control, Notch2KD, and Notch3KD) (Scale bar=50µm) and histograms (C) depicting the

intensity histograms of the SMCs based on flow cytometry. The bar plots (D) show the fold change in mean intensity of the live cells stained with J1-Fc measured using flow cytometry (mean+SD, n=3 independent experiments, one-way ANOVA followed by Šídák's test for multiple comparisons. Pairwise comparisons between J1-Fc-stained samples with p values lower than 0.1 are shown on the plot.).

(E, F) Immunoblots produced by C-terminal probing of Notch2 and Notch3 following DAPT washout in SMCs plated on immobilized J1-Fc, and the quantitative analysis of the bands. The receptor cleavage was measured by the ratio of the NEXT (lower band) to the total S1-processed fragment (NEXT+TMIC (higher band)) (mean+SD, n=3 independent experiments, one-way ANOVA followed by Šídák's test for multiple comparisons. Pairwise comparisons with p values lower than 0.1 are shown on the plot.).

(G,H) CSL-dependent Notch transcriptional activity in HEK 293T cells transfected with increasing amounts of Flag-tagged Notch2 or Notch3 ICD and 12xCSL-luciferase (G). The luciferase activity is presented as luminescence intensity relative to β-galactosidase activity (mean+SD, n=3 independent experiments. Data are presented as regression curves and circles as replicates.). (H) Immnunoblots indicating efficient transfection of the NICD-flag constructs.

(I, J) Flag-tagged NICD paralogs were immunoprecipitated from HEK 293T cells co-expressing 6xHis-tagged RBPJκ (I). The Flag and the 6xHis IP signals were normalized to the input. The normalized 6xHis/Flag signal is presented in the bar plot (J) (mean+SD, n=3 independent experiments, one-way ANOVA followed by Tukey's test for multiple comparisons. Pairwise comparisons between NICD paralogs with p values lower than 0.1 are shown on the plot.).

688

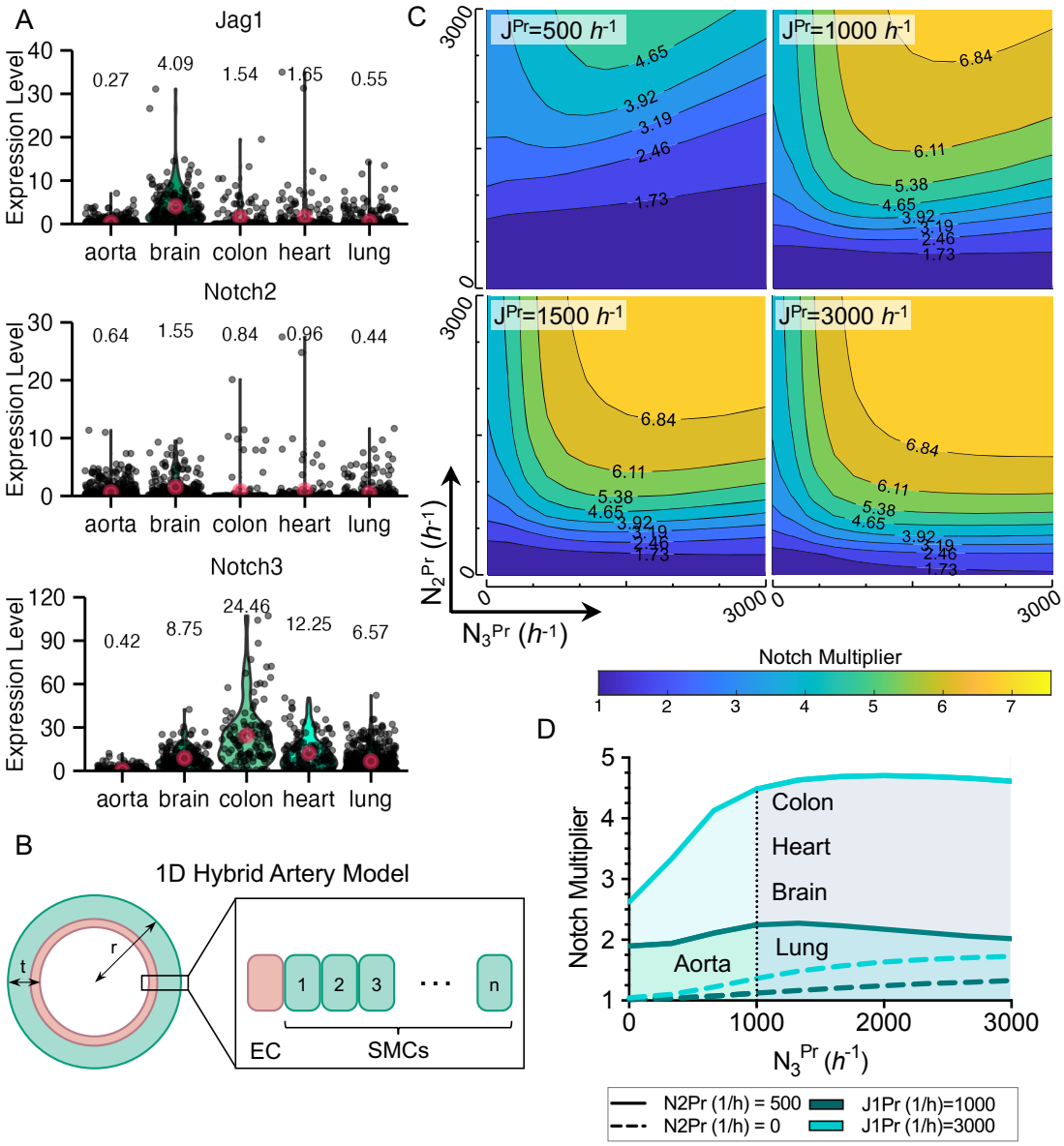

689

690 **Figure 4. Levels of Notch3 predict artery-typical vulnerability to altered Jagged1-**

691 **Notch2/Notch3 signaling in the SMCs.**

692 (A) Normalized expression of Jag1, Notch2, and Notch3 in arterial SMCs of different mouse

693 organs extracted from scRNAseq data (Muhl et al.(35); aorta, heart, colon, and lung) and

694 (Vanlandewijck et al.(57); brain). The circles and the text above the violin plots denote the mean
695 expression.
696 (B) Schematic one-dimensional array of 1D artery model with an endothelial cell and a row of
697 SMCs. The cascade of signaling is initiated by constant Jagged1 emission from the endothelial
698 cell (EC) and SMCs are interacting with their neighboring cells.
699 (C) Heatmaps showing the simulated impact of the initial Jagged1, Notch2, and Notch3 levels
700 on the Notch signaling readout (Notch multiplier) in the 1D hybrid arterial wall.
701 (D) 2D projection of the predicted ranges of Notch multiplier in arterial SMCs of different organs
702 with respect to their stoichiometrically scaled levels of Jagged1, Notch2, and Notch3 based on
703 A, and in a Notch2 knockout scenario.

704

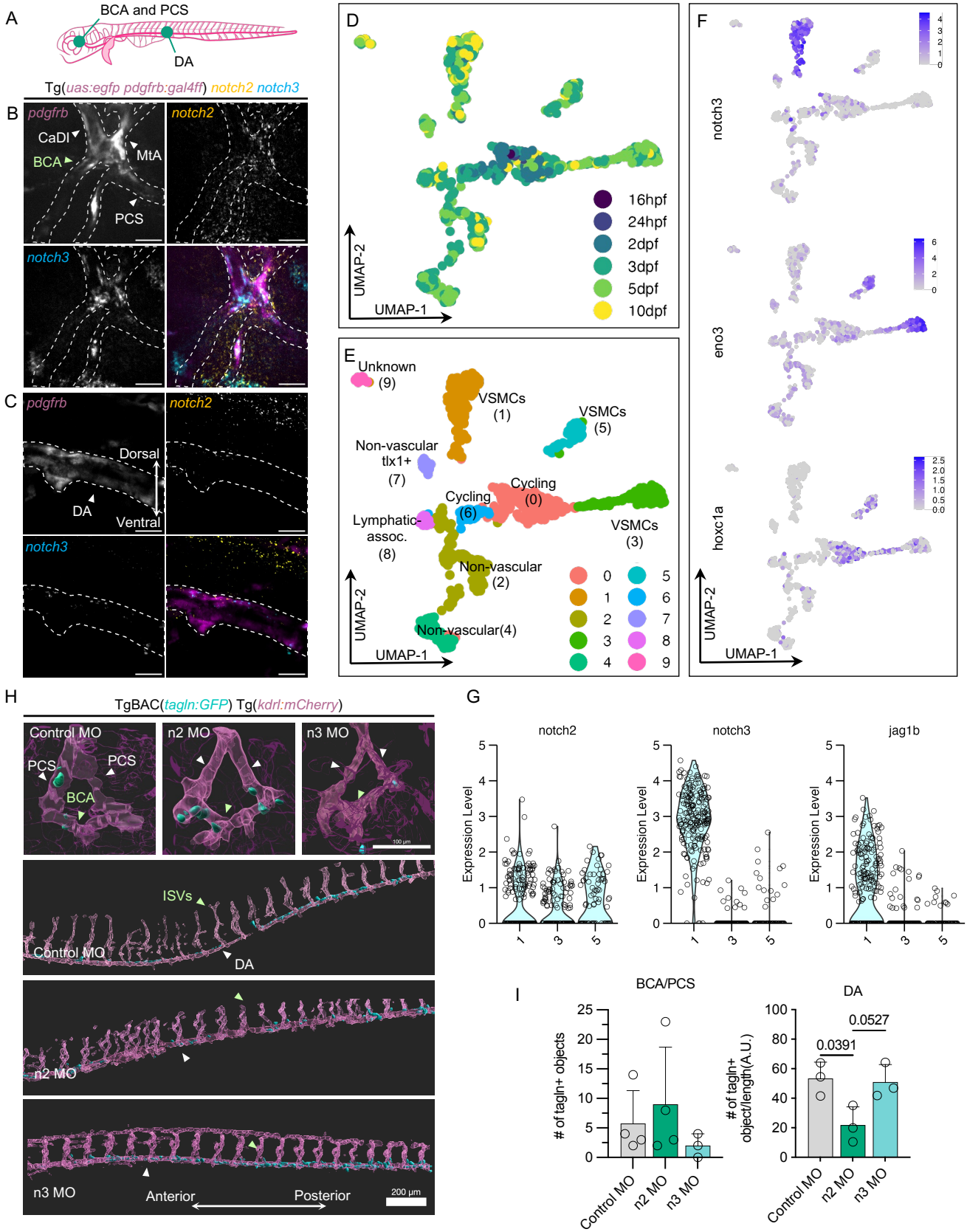
A
BCA and PCS
DA
Tg(uas:egfp pdgfrb:gal4ff) notch2 notch3
B
pdgfrb
CaDI
BCA
MtA
PCS
notch2
notch3
C
pdgfrb
Dorsal
DA
Ventral
notch2
notch3
D
16hpf
24hpf
2dpf
3dpf
5dpf
10dpf
UMAP-2
UMAP-1
E
Unknown (9)
VSMCs (1)
VSMCs (5)
Non-vascular tlx1+ (7)
Cycling (0)
Cycling (6)
Lymphatic assoc. (8)
VSMCs (3)
Non-vascular (2)
Non-vascular(4)
UMAP-2
UMAP-1
F
notch3
eno3
hoxc1a
UMAP-2
UMAP-1
H
TgBAC(tagln:GFP) Tg(kdrl:mCherry)
Control MO
PCS
PCS
BCA
n2 MO
n3 MO
ISVs
Control MO
DA
n2 MO
n3 MO
Anterior
Posterior
200 µm
G
notch2
notch3
jag1b
Expression Level
I
BCA/PCS
# of tagln+ objects
Control MO
n2 MO
n3 MO
DA
# of tagln+ object/length(A.U.)
0.0391
0.0527

705 **Figure 5: Developing SMCs at the cerebral base can compensate Notch2 depletion in the**
706 **zebrafish larvae.**
707 *(A) Schematic description of the vascular tree of the zebrafish larvae, and the position of the*
708 *DA, the PCS, and the BCA (Created using Biorender).*
709 *(B, C) In situ RNA HCR was performed with probes against notch2 and notch3 in 3dpf zebrafish*
710 *larvae bearing a pdgfrb reporter. Confocal sections of the arteries from the cerebral base (B)*
711 *and the dorsal aorta (C) given with dashed lines loosely marking the arterial regions based on*
712 *the pdgfrb signal are shown (Scale bars=20 µm) (DA: dorsal aorta, BCA: basal communicating*
713 *artery, PCS: posterior communicating segment, CaDI: caudal division of the internal carotid*
714 *artery, MtA: metencephalic artery)*
715 *(D, E) UMAP projection of the SMCs color-coded based on the Seurat clusters and the*
716 *developmental stage from the Zebrahub mesoderm scRNAseq dataset. Cluster annotations*
717 *were based on known markers of vascular and non-vascular SMCs as well as notch3*
718 *expression (Please also see Fig. 4S for the markers used for annotation).*
719 *(F, G) Normalized expression of notch3, trunk marker eno3, and anteroposterior position-related*
720 *homeobox gene hoxc1a (Color gradient denotes log-normalized expression.); and (G) the*
721 *normalized expression of the Notch signaling components in the indicated vascular SMC*
722 *clusters.*
723 *(H, I) The embryos bearing a contractility reporter (tagln:GFP) or the endothelial reporter*
724 *(kdrl:mCherry) were injected with 10ng control, notch2 or notch3 morpholinos. The orthogonal*
725 *view of the surface-rendered light sheet images of the indicated arteries from the 102 hpf (H,*
726 *the BCA/PCS, scale bar=100µm and H, the DA and the ISV, scale bar=200µm). The number of*
727 *tagln+ objects associated with the endothelium are shown in the bar plots (I) (mean+SD, n=3 or*
728 *4 embryos per morphant group, one-way ANOVA followed by Tukey´s test for multiple*
729 *comparisons. Pairwise comparisons with p values smaller than 0.1 are shown on the plots.).*

REFERENCES

1. M. Hellström, M. Kalén, P. Lindahl, A. Abramsson, C. Betsholtz, Role of PDGF-B and PDGFR-β in recruitment of vascular smooth muscle cells and pericytes during embryonic blood vessel formation in the mouse. *Development* **126**, 3047–3055 (1999).

2. J. E. Wagenseil, R. P. Mecham, Vascular Extracellular Matrix and Arterial Mechanics. *Physiological Reviews* **89**, 957–989 (2009).

3. C. Yap, A. Mieremet, C. J. M. de Vries, D. Micha, V. de Waard, Six Shades of Vascular Smooth Muscle Cells Illuminated by KLF4 (Krüppel-Like Factor 4). *Arteriosclerosis, Thrombosis, and Vascular Biology* **41**, 2693–2707 (2021).

4. J. T. Baeten, B. Lilly, Notch Signaling in Vascular Smooth Muscle Cells. *Adv Pharmacol* **78**, 351–382 (2017).

5. C. Siebel, U. Lendahl, Notch Signaling in Development, Tissue Homeostasis, and Disease. *Physiological Reviews* **97**, 1235–1294 (2017).

6. F. Suarez Rodriguez, S. Sanlidag, C. Sahlgren, Mechanical regulation of the Notch signaling pathway. *Current Opinion in Cell Biology* **85**, 102244 (2023).

7. M. Sjöqvist, E. R. Andersson, Do as I say, Not(ch) as I do: Lateral control of cell fate. *Developmental Biology* **447**, 58–70 (2019).

8. S. Jin, *et al.*, Notch Signaling Regulates Platelet-Derived Growth Factor Receptor-β Expression in Vascular Smooth Muscle Cells. *Circulation Research* **102**, 1483–1491 (2008).

9. K. Ando, *et al.*, Peri-arterial specification of vascular mural cells from naïve mesenchyme requires Notch signaling. *Development* **146**, dev165589 (2019).

10. Q. Wang, N. Zhao, S. Kennard, B. Lilly, Notch2 and Notch3 Function Together to Regulate Vascular Smooth Muscle Development. *PLOS ONE* **7**, e37365 (2012).

11. J. M. Boucher, A. Harrington, B. Rostama, V. Lindner, L. Liaw, A Receptor-Specific Function for Notch2 in Mediating Vascular Smooth Muscle Cell Growth Arrest Through Cyclin-dependent Kinase Inhibitor 1B. *Circulation Research* **113**, 975–985 (2013).

12. L. J. Manderfield, *et al.*, Notch activation of Jagged1 contributes to the assembly of the arterial wall. *Circulation* **125**, 314–323 (2012).

13. S. Loerakker, *et al.*, Mechanosensitivity of Jagged–Notch signaling can induce a switch-type behavior in vascular homeostasis. *Proceedings of the National Academy of Sciences* **115**, E3682–E3691 (2018).

762 14. T. Ristori, O. M. J. A. Stassen, C. M. Sahlgren, S. Loerakker, Lateral induction limits the
763 impact of cell connectivity on Notch signaling in arterial walls. *International Journal for*
764 *Numerical Methods in Biomedical Engineering* **36**, e3323 (2020).

765 15. M. A. Gilbert, *et al.*, Alagille syndrome mutation update: Comprehensive overview of
766 JAG1 and NOTCH2 mutation frequencies and insight into missense variant
767 classification. *Hum Mutat* **40**, 2197–2220 (2019).

768 16. D. B. McElhinney, *et al.*, Analysis of Cardiovascular Phenotype and Genotype-
769 Phenotype Correlation in Individuals With a JAG1 Mutation and/or Alagille Syndrome.
770 *Circulation* **106**, 2567–2574 (2002).

771 17. K. M. Emerick, *et al.*, Intracranial Vascular Abnormalities in Patients with Alagille
772 Syndrome. *Journal of Pediatric Gastroenterology and Nutrition* **41**, 99–107 (2005).

773 18. S.-M. Yuan, Pulmonary artery pathologies in Alagille syndrome: a meta-analysis.
774 *Postepy Kardiol Interwencyjnej* **18**, 111–117 (2022).

775 19. Y. Zhang, *et al.*, JAGGED-NOTCH3 signaling in vascular remodeling in pulmonary
776 arterial hypertension. *Science Translational Medicine* **14**, eabl5471 (2022).

777 20. R. Okeda, K. Arima, M. Kawai, Arterial Changes in Cerebral Autosomal Dominant
778 Arteriopathy With Subcortical Infarcts and Leukoencephalopathy (CADASIL) in
779 Relation to Pathogenesis of Diffuse Myelin Loss of Cerebral White Matter. *Stroke* **33**,
780 2565–2569 (2002).

781 21. A. Joutel, *et al.*, Notch3 mutations in CADASIL, a hereditary adult-onset condition
782 causing stroke and dementia. *Nature* **383**, 707–710 (1996).

783 22. F. A. High, *et al.*, Endothelial expression of the Notch ligand Jagged1 is required for
784 vascular smooth muscle development. *Proc Natl Acad Sci U S A* **105**, 1955–1959
785 (2008).

786 23. P. Varadkar, *et al.*, Notch2 is required for the proliferation of cardiac neural crest-
787 derived smooth muscle cells. *Developmental Dynamics* **237**, 1144–1152 (2008).

788 24. J. T. Baeten, A. R. Jackson, K. M. McHugh, B. Lilly, Loss of Notch2 and Notch3 in
789 vascular smooth muscle causes patent ductus arteriosus. *Genesis* **53**, 738–748
790 (2015).

791 25. A. Granata, *et al.*, Temporal and Embryonic Lineage-Dependent Regulation of Human
792 Vascular SMC Development by NOTCH3. *Stem Cells and Development* **24**, 846–856
793 (2015).

794 26. K. S. Volz, *et al.*, Pericytes are progenitors for coronary artery smooth muscle. *eLife* **4**,
795 e10036.

796 27. V. Domenga, *et al.*, Notch3 is required for arterial identity and maturation of vascular
797 smooth muscle cells. *Genes Dev* **18**, 2730–2735 (2004).

798 28. E. J. B. de Chantemèle, *et al.*, Notch3 is a major regulator of vascular tone in cerebral
799 and tail resistance arteries. *Arterioscler Thromb Vasc Biol* **28**, 2216–2224 (2008).

800 29. T. L. Henshall, *et al.*, Notch3 Is Necessary for Blood Vessel Integrity in the Central
801 Nervous System. *Arteriosclerosis, Thrombosis, and Vascular Biology* **35**, 409–420
802 (2015).

803 30. J. T. Baeten, B. Lilly, Differential Regulation of NOTCH2 and NOTCH3 Contribute to Their
804 Unique Functions in Vascular Smooth Muscle Cells. *J Biol Chem* **290**, 16226–16237
805 (2015).

806 31. J. M. Dave, *et al.*, JAGGED1/NOTCH3 activation promotes aortic hypermuscularization
807 and stenosis in elastin deficiency. *J Clin Invest* **132** (2022).

808 32. S. Kapuria, *et al.*, Heterogeneous pdgfrb+ cells regulate coronary vessel development
809 and revascularization during heart regeneration. *Development* **149**, dev199752 (2022).

810 33. N. J. Leeper, *et al.*, Loss of CDKN2B Promotes p53-Dependent Smooth Muscle Cell
811 Apoptosis and Aneurysm Formation. *Arteriosclerosis, Thrombosis, and Vascular*
812 *Biology* **33**, e1–e10 (2013).

813 34. E. Murayama, C. Vivier, A. Schmidt, P. Herbomel, Alcam-a and Pdgfr-α are essential for
814 the development of sclerotome-derived stromal cells that support hematopoiesis.
815 *Nat Commun* **14**, 1171 (2023).

816 35. L. Muhl, *et al.*, A single-cell transcriptomic inventory of murine smooth muscle cells.
817 *Dev Cell* **57**, 2426-2443.e6 (2022).

818 36. M. Ainiwan, Q. Wang, G. Yesitayi, X. Ma, Identification of FERMT1 and SGCD as key
819 marker in acute aortic dissection from the perspective of predictive, preventive, and
820 personalized medicine. *EPMA J* **13**, 597–614 (2022).

821 37. D. Klessinger, *et al.*, Divergent and Compensatory Effects of BMP2 and BMP4 on the
822 VSMC Phenotype and BMP4's Role in Thoracic Aortic Aneurysm Development. *Cells*
823 **13**, 735 (2024).

824 38. D. Morrow, *et al.*, Notch-mediated CBF-1/RBP-Jκ-dependent regulation of human
825 vascular smooth muscle cell phenotype in vitro. *American Journal of Physiology-Cell*
826 *Physiology* **289**, C1188–C1196 (2005).

827 39. H. Doi, *et al.*, Jagged1-selective Notch Signaling Induces Smooth Muscle Differentiation
828 via a RBP-Jκ-dependent Pathway *. *Journal of Biological Chemistry* **281**, 28555–28564
829 (2006).

830 40. N. Shi, X. Guo, S.-Y. Chen, Olfactomedin 2, a novel regulator for transforming growth
831 factor-β–induced smooth muscle differentiation of human embryonic stem cell–
832 derived mesenchymal cells. *Mol Biol Cell* **25**, 4106–4114 (2014).

833 41. N. Shi, C.-X. Li, X.-B. Cui, S. I. Tomarev, S.-Y. Chen, Olfactomedin 2 Regulates Smooth
834 Muscle Phenotypic Modulation and Vascular Remodeling Through Mediating Runt-
835 Related Transcription Factor 2 Binding to Serum Response Factor. *Arteriosclerosis,*
836 *Thrombosis, and Vascular Biology* **37**, 446–454 (2017).

837 42. L.-H. Zhu, *et al.*, Mindin regulates vascular smooth muscle cell phenotype and prevents
838 neointima formation. *Clinical Science* **129**, 129–145 (2015).

839 43. M. Heglind, *et al.*, Lack of the Central Nervous System- and Neural Crest-Expressed
840 Forkhead Gene Foxs1 Affects Motor Function and Body Weight. *Mol Cell Biol* **25**,
841 5616–5625 (2005).

842 44. Y. Sato, *et al.*, Importance of forkhead transcription factor Fkhl18 for development of
843 testicular vasculature. *Molecular Reproduction and Development* **75**, 1361–1371
844 (2008).

845 45. E. A. Bates, *et al.*, FOXS1 is increased in liver fibrosis and regulates TGFβ
846 responsiveness and proliferation pathways in human hepatic stellate cells. *Journal of*
847 *Biological Chemistry* **300** (2024).

848 46. A. B. Keenan, *et al.*, ChEA3: transcription factor enrichment analysis by orthogonal
849 omics integration. *Nucleic Acids Res* **47**, W212–W224 (2019).

850 47. H. Liu, S. Kennard, B. Lilly, NOTCH3 Expression Is Induced in Mural Cells Through an
851 Autoregulatory Loop That Requires Endothelial-Expressed JAGGED1. *Circulation*
852 *Research* **104**, 466–475 (2009).

853 48. N. Zhao, H. Liu, B. Lilly, Reciprocal Regulation of Syndecan-2 and Notch Signaling in
854 Vascular Smooth Muscle Cells *. *Journal of Biological Chemistry* **287**, 16111–16120
855 (2012).

856 49. H. Meng, X. Zhang, K. D. Hankenson, M. M. Wang, Thrombospondin 2 Potentiates
857 Notch3/Jagged1 Signaling. *J Biol Chem* **284**, 7866–7874 (2009).

858 50. C. Mao, *et al.*, Nidogen-2 Maintains the Contractile Phenotype of Vascular Smooth
859 Muscle Cells and Prevents Neointima Formation via Bridging Jagged1-Notch3
860 Signaling. *Circulation* **144**, 1244–1261 (2021).

861 51. Z. Liu, *et al.*, The extracellular domain of Notch2 increases its cell-surface abundance
862 and ligand responsiveness during kidney development. *Dev Cell* **25**, 585–598 (2013).

863 52. X. Xu, *et al.*, Insights into Autoregulation of Notch3 from Structural and Functional
864 Studies of Its Negative Regulatory Region. *Structure* **23**, 1227–1235 (2015).

865 53. A. J. Groot, *et al.*, Regulated Proteolysis of NOTCH2 and NOTCH3 Receptors by ADAM10
866 and Presenilins. *Mol Cell Biol* **34**, 2822–2832 (2014).

867 54. R. A. J. Habets, *et al.*, Human NOTCH2 Is Resistant to Ligand-independent Activation by
868 Metalloprotease Adam17. *J Biol Chem* **290**, 14705–14716 (2015).

869 55. S. K. J. Landor, *et al.*, PIM-induced phosphorylation of Notch3 promotes breast cancer
870 tumorigenicity in a CSL-independent fashion. *Journal of Biological Chemistry* **296**
871 (2021).

872 56. Z. Liu, *et al.*, The intracellular domains of Notch1 and Notch2 are functionally
873 equivalent during development and carcinogenesis. *Development* **142**, 2452–2463
874 (2015).

875 57. M. Vanlandewijck, *et al.*, A molecular atlas of cell types and zonation in the brain
876 vasculature. *Nature* **554**, 475–480 (2018).

877 58. L. Muhl, *et al.*, A single-cell transcriptomic inventory of murine smooth muscle cells.
878 *Dev Cell* **57**, 2426-2443.e6 (2022).

879 59. M. C. Romay, *et al.*, Region-specific gene expression and sex inform about disease
880 susceptibility in the aorta. *Nat Cardiovasc Res* **4**, 1152–1171 (2025).

881 60. L. He, *et al.*, Single-cell RNA sequencing of mouse brain and lung vascular and vessel-
882 associated cell types. *Sci Data* **5**, 180160 (2018).

883 61. N. C. A. van Engeland, *et al.*, Vimentin regulates Notch signaling strength and arterial
884 remodeling in response to hemodynamic stress. *Sci Rep* **9**, 12415 (2019).

885 62. J. G. M. van Asten, *et al.*, Computational analysis of the role of mechanosensitive Notch
886 signaling in arterial adaptation to hypertension. *Journal of the Mechanical Behavior of*
887 *Biomedical Materials* **133**, 105325 (2022).

888 63. J. G. M. van Asten, *et al.*, A multiscale computational model of arterial growth and
889 remodeling including Notch signaling. *Biomech Model Mechanobiol* **22**, 1569–1588
890 (2023).

891 64. B. McCright, J. Lozier, T. Gridley, A mouse model of Alagille syndrome: Notch2 as a
892 genetic modifier of Jag1 haploinsufficiency. *Development* **129**, 1075–1082 (2002).

893 65. A. Briot, *et al.*, Repression of Sox9 by Jag1 Is Continuously Required to Suppress the
894 Default Chondrogenic Fate of Vascular Smooth Muscle Cells. *Developmental Cell* **31**,
895 707–721 (2014).

896 66. F. A. High, *et al.*, Endothelial expression of the Notch ligand Jagged1 is required for
897 vascular smooth muscle development. *Proc Natl Acad Sci U S A* **105**, 1955–1959
898 (2008).

899 67. S. I. Travisano, *et al.*, Coronary arterial development is regulated by a Dll4-Jag1-
900 EphrinB2 signaling cascade. *eLife* **8**, e49977 (2019).

901 68. X. Feng, L. T. Krebs, T. Gridley, Patent ductus arteriosus in mice with smooth muscle-
902 specific Jag1 deletion. *Development* **137**, 4191–4199 (2010).

903 69. B. M. Hogan, S. Schulte-Merker, How to Plumb a Pisces: Understanding Vascular
904 Development and Disease Using Zebrafish Embryos. *Developmental Cell* **42**, 567–583
905 (2017).

906 70. M. Lange, *et al.*, A multimodal zebrafish developmental atlas reveals the state-
907 transition dynamics of late-vertebrate pluripotent axial progenitors. *Cell* **187**, 6742-
908 6759.e17 (2024).

909 71. K. Ando, T. Ishii, S. Fukuhara, Zebrafish Vascular Mural Cell Biology: Recent Advances,
910 Development, and Functions. *Life* **11**, 1041 (2021).

911 72. Y. Hao, *et al.*, Integrated analysis of multimodal single-cell data. *Cell* **184**, 3573-
912 3587.e29 (2021).

913 73. T. R. Whitesell, *et al.*, *foxc1* is required for embryonic head vascular smooth muscle
914 differentiation in zebrafish. *Developmental Biology* **453**, 34–47 (2019).

915 74. K. Ando, *et al.*, KCNJ8/ABCC9-containing K-ATP channel modulates brain vascular
916 smooth muscle development and neurovascular coupling. *Developmental Cell* **57**,
917 1383-1399.e7 (2022).

918 75. J. C.-G. Hombría, M. García-Ferrés, C. Sánchez-Higueras, Anterior Hox Genes and the
919 Process of Cephalization. *Front. Cell Dev. Biol.* **9** (2021).

920 76. M. C. Romay, *et al.*, Age-related loss of Notch3 underlies brain vascular contractility
921 deficiencies, glymphatic dysfunction, and neurodegeneration in mice. *J Clin Invest*
922 **134** (2024).

923 77. L. Choy, *et al.*, Constitutive NOTCH3 Signaling Promotes the Growth of Basal Breast
924 Cancers. *Cancer Research* **77**, 1439–1452 (2017).

925 78. R. R. Arasada, *et al.*, Notch3-dependent β-catenin signaling mediates EGFR TKI drug
926 persistence in EGFR mutant NSCLC. *Nat Commun* **9**, 3198 (2018).

927 79. B. McCright, J. Lozier, T. Gridley, Generation of new Notch2 mutant alleles. *genesis* **44**,
928 29–33 (2006).

929 80. S. M. Peterson, *et al.*, Notch2 and Proteomic Signatures in Mouse Neointimal Lesion
930 Formation. *Arteriosclerosis, Thrombosis, and Vascular Biology* **38**, 1576–1593 (2018).

931 81. J. Davis-Knowlton, J. E. Turner, A. Harrington, L. Liaw, Smooth Muscle Cell Notch2 Is
932 Not Required for Atherosclerotic Plaque Formation in ApoE Null Mice. *Journal of*
933 *Vascular Research* **59**, 261–274 (2022).

934 82. Y. Li, *et al.*, Smooth Muscle Notch1 Mediates Neointimal Formation After Vascular
935 Injury. *Circulation* **119**, 2686–2692 (2009).

936 83. A. I. Machuca-Parra, *et al.*, Therapeutic antibody targeting of Notch3 signaling prevents
937 mural cell loss in CADASIL. *Journal of Experimental Medicine* **214**, 2271–2282 (2017).

938 84. A. Joutel, *et al.*, Strong clustering and stereotyped nature of Notch3 mutations in
939 CADASIL patients. *The Lancet* **350**, 1511–1515 (1997).

940 85. A. Joutel, *et al.*, The ectodomain of the Notch3 receptor accumulates within the
941 cerebrovasculature of CADASIL patients. *J Clin Invest* **105**, 597–605 (2000).

942 86. M. Monet-Leprêtre, *et al.*, Abnormal recruitment of extracellular matrix proteins by
943 excess Notch3ECD: a new pathomechanism in CADASIL. *Brain* **136**, 1830–1845
944 (2013).

945 87. E. R. Andersson, *et al.*, Mouse Model of Alagille Syndrome and Mechanisms of Jagged1
946 Missense Mutations. *Gastroenterology* **154**, 1080–1095 (2018).

947 88. S. Hankeova, *et al.*, Sex differences and risk factors for bleeding in Alagille syndrome.
948 *EMBO Mol Med* **14**, e15809 (2022).

949 89. N. Dupré, *et al.*, Protein aggregates containing wild-type and mutant NOTCH3 are major
950 drivers of arterial pathology in CADASIL. *J Clin Invest* **134** (2024).

951 90. C. Karakaya, *et al.*, Notch signaling regulates strain-mediated phenotypic switching of
952 vascular smooth muscle cells. *Front. Cell Dev. Biol.* **10** (2022).

953 91. N. Nandagopal, *et al.*, Dynamic Ligand Discrimination in the Notch Signaling Pathway.
954 *Cell* **172**, 869-880.e19 (2018).

955 92. F. Bernard, A. Krejci, B. Housden, B. Adryan, S. J. Bray, Specificity of Notch pathway
956 activation: Twist controls the transcriptional output in adult muscle progenitors.
957 *Development* **137**, 2633–2642 (2010).

958 93. L. L. O'Brien, *et al.*, Wt1a, Foxc1a, and the Notch mediator Rbpj physically interact and
959 regulate the formation of podocytes in zebrafish. *Developmental Biology* **358**, 318–330
960 (2011).

961 94. J. Sachdeva, *et al.*, Smooth muscle cell-specific Notch1 haploinsufficiency restricts the
962 progression of abdominal aortic aneurysm by modulating CTGF expression. *PLoS ONE*
963 **12**, e0178538 (2017).

964 95. D. Antfolk, *et al.*, Selective regulation of Notch ligands during angiogenesis is mediated
965 by vimentin. *Proceedings of the National Academy of Sciences* **114**, E4574–E4581
966 (2017).

967 96. H. M. T. Choi, *et al.*, Third-generation in situ hybridization chain reaction: multiplexed,
968 quantitative, sensitive, versatile, robust. *Development* **145**, dev165753 (2018).

969 97. J. Schindelin, *et al.*, Fiji: an open-source platform for biological-image analysis. *Nat*
970 *Methods* **9**, 676–682 (2012).

971 98. M. Boareto, *et al.*, Jagged–Delta asymmetry in Notch signaling can give rise to a
972 Sender/Receiver hybrid phenotype. *Proc. Natl. Acad. Sci. U.S.A.* **112** (2015).

973 99. T. Konishi, *et al.*, The histological analysis of the coronary medial thickness:
974 Implications for percutaneous coronary intervention. *PLOS ONE* **18**, e0283840 (2023).

975

Supporting Information for

Receptor stoichiometry predicts artery-typical vulnerability to altered Notch signaling during smooth muscle differentiation.

Sami Sanlidag[1,2,3], Noora Virtanen[1,2,3,a], Hesam Hoursan[4,5,a], Tommaso Ristori[4,5], Marika Sjöqvist[1,2], Sandra Loerakker[4,5], Cecilia Sahlgren[1,2,3,4,5,6]

[1]Faculty of Science and Engineering, Cell Biology, Åbo Akademi University, Tykistökatu 6, FI-20520, Turku, Finland

[2]Turku Bioscience, Åbo Akademi University and University of Turku, Tykistökatu 6, FI-20520, Turku, Finland

[3]InFLAMES Research Flagship Center, Åbo Akademi University and University of Turku, Turku, Finland

[4]Department of Biomedical Engineering, Eindhoven University of Technology, PO Box 513, 5600 MB, Eindhoven, the Netherlands

[5]Institute for Complex Molecular Systems (ICMS), Eindhoven University of Technology, Ceres, Building Number 7, De Zaale, 5612 AJ, Eindhoven, the Netherlands

[a] These authors contributed equally.

[6]Lead contact (Cecilia.sahlgren@abo.fi).

Contents:

Supporting Methods

Figures S1 to S4

Table S1 to S4

SI References

Other supporting materials for this manuscript include the following:

Dataset S1

1000 **Supporting Information Text**

1001 **Supporting Methods**

1002 Cell Culture and Maintenance

1003 Human aortic smooth muscle cells (SMCs) were purchased from Lonza (Cat. #CC-2571) and American
1004 Type Culture Collection (ATCC Cat. #PCS-100-012) in passages 3 or 2 (See Table S4 for details). The cells
1005 were grown in Smooth Muscle Basal Medium containing SmGM®-2 SingleQuots supplements (Lonza Cat.
1006 #CC-3182) until passage 4-6 and used within 15 population doublings. Human umbilical vein endothelial
1007 cells (HUVECs) were bought from PromoCell (Cat. #C-12200) at passage 1 and grown in Endothelial Cell
1008 Growth Medium 2 (PromoCell Cat.#C-22011) until passage number 4. Human embryonic kidney cell line
1009 HEK 293T was grown in Dulbecco´s Modified Eagle´s Medium (Merck Cat. #D6429) supplemented with
1010 10% fetal bovine serum (Gibco Cat. #17914671), 2 mM L-glutamine (Merck Cat. #G7513) and 100 units/ml
1011 penicillin/streptomycin (Merck Cat. #P0781). All cells were maintained at 37°C with 5% CO_2 and kept under
1012 80% confluency at all times unless the experimental setting required otherwise.

1013 Ligand Coating

1014 For the Notch activation assays, the recombinant human Jagged1-Fc chimeric ligands (Bio-techne Cat.
1015 #1277-JG) were immobilized on the culture plates at 10nM concentration as described previously(1). Briefly,
1016 the culture plates were first treated with 50µg/ml protein G (Thermo Fisher Scientific Cat. #21193) in
1017 phosphate-buffered saline (PBS) (Biowest Cat. #L0616) overnight at RT. The next day, the plates were
1018 washed three times with PBS and blocked with 1% bovine serum albumin (BSA) (Merck Cat. #A9418) in
1019 PBS for 1 hour at RT. Then, the plates were treated with the ligands in PBS with 0.1% BSA overnight at
1020 cold or 2 hours at RT. The plates were washed three times with PBS before use.

1021 RNA interference and Plasmids

1022 For siRNA transfections, 10^4 SMCs per cm^2 were plated in 6cm culture dishes and grown overnight. The
1023 next morning, the cells were transfected with 25nM Dharmacon ON-TARGETplus SMARTPool siRNAs
1024 (Horizon Discovery) for the indicated genes or with the same concentration of non-targeting siRNA (Eurofins
1025 Genomics) using RNAiMAX lipofectamine (Thermo Fisher Scientific Cat. #13778150). Briefly, the siRNAs
1026 and the lipofectamine solutions were separately prepared in Opti-MEM (Gibco Cat. #31985062). The
1027 lipofectamine solution was dropwise added to the siRNA solution and mixed gently by flicking the tubes.
1028 The solution was then briefly centrifuged and left to incubate for 15 min at RT. The cells were supplied with
1029 fresh growth media. The siRNA mix was dropwise added to the culture plate and swirled gently to mix. The
1030 cells were then incubated for 24 or 48 hours according to the experimental setting before use. 10

1031 For plasmid transfection, HEK 293T cells were grown to 70% confluence in 10 cm culture dishes. The
1032 indicated plasmids were transfected using jetOPTIMUS transfection kit (Sartorius Cat. #101000006) at
1033 1µg/ml concentration, according to the supplier´s recommendations. Briefly, the plasmids and the
1034 transfection reagent were added to the supplied buffer and mixed using a vortex for 1 second. The tube
1035 was centrifuged for 10 s and left to incubate for 10 min. The solution was then dropwise added to the culture
1036 plate that was supplied with fresh, warm media. The cells were then incubated overnight before use.

1037 Fixation and mounting for microscopy

1038 The cells were washed three times with HBS, fixed with 4% PFA in PBS for 10 min at RT, and mounted
1039 using Vectashield with DAPI (4',6-diamidino-2-phenylindole, dihydrochloride) (Vector Laboratories Cat. #H-
1040 1000). The samples were imaged using the 3i CSU-W1 spinning disc confocal microscope.

1041 Flow cytometry

1042 The cells were washed three times with HBS and detached using ReagentPack™ subculture reagents
1043 (Lonza Cat. #CC50-34) at RT and immediately taken on ice and collected into 1.5 ml centrifuge tubes. The
1044 cells were washed with ice-cold HBS three times by centrifuging for 3 min at 500 RCF, 4°C, and
1045 resuspending in fresh buffer. The cells were analyzed with BD LSR Fortessa flow cytometer using 488 nm
1046 excitation wavelength. The data were analyzed using the FlowJo software (v.10) and presented as mean
1047 fluorescence intensity.

1048 Spheroid formation

1049 $8x10^3$ SMCs were grown in Nuncleon™ Sphera™ low adhesion plates (Thermo Fisher Scientific Cat.
1050 #174929) for 72 hours in SMGM-2 media to form mono-culture SMC spheroids. For the co-culture
1051 spheroids, SMCs were first grown for 48 hours alone and then for 24 hours with $3x10^3$ HUVECs. The
1052 spheroids were washed once with PBS, then fixed and permeabilized in PBS containing 4%
1053 paraformaldehyde and 1% Triton X-100 (VWR, Cat. #M143) overnight at cold. They were washed three
1054 times for 15 min each in PBS with 0.1% Triton X-100 and incubated with 1:100 mouse CD31 (Thermo Fisher
1055 Scientific Cat. #37-0700) and 1:100 rabbit Jagged1 (Cell Signaling Cat. #2620) primary antibodies overnight
1056 at cold. The spheroids were washed three times and incubated with 1:400 dilutions of the anti-rabbit Alexa
1057 fluor 488 (Thermo Fisher Scientific Cat. #A-11034) and anti-mouse Alexa fluor 555 antibodies (Thermo
1058 Fisher Scientific Cat. #A-21422). After three more washes, the spheroids were mounted in glycerol (Merck
1059 Cat. #G5516). The samples were imaged using the 3i CSU-W1 spinning disc confocal microscope. The
1060 mean Jagged1 signal in confocal slices from the middle of the spheroids was quantified using Fiji ImageJ
1061 and normalized by subtracting the intensity of the control samples without primary antibodies. At least four
1062 spheroids were analyzed per group for each independent experiment. The normalized signal was presented
1063 as a fold change.

1064 RNA isolation, cDNA synthesis, and qPCR

1065 RNA was isolated from SMCs using NucleoSpin RNA (Macharey-Nagel Cat. #740955) according to the
1066 supplier´s protocol. The RNA concentration and quality were checked using Nanodrop ND-2000, Thermore
1067 Fisher Scientific. The resulting RNA was used for cDNA library preparation using the SensiFAST™ cDNA
1068 synthesis kit (Bioline Cat. #BIO-65054). The quantitative polymerase chain reaction (qPCR) using 5x HOT
1069 FIREPol EvaGreen qPCR Mix Plus reagent (Labnet Cat. #08-24-00001-10) according to the supplier´s
1070 protocol using Quanstudio Real-Time PCR system, Thermo Fisher Scientific. The qPCR primers for the
1071 indicated genes were ordered from TAG Copenhagen (See the Table S2 for the primer sequences). For all
1072 primer pairs, a cDNA dilution series, prepared from a cocktail of samples from the same experiment, was
1073 included in the same qPCR run to calculate a standard curve. The standard curve was used to calculate
1074 the relative mRNA expression.

1075 RNA Sequencing and Data Processing

1076 For each sample, a starting quantity of 100 ng RNA was processed. Sample quality was ensured using
1077 Agilent BioAnalyzer 2100. Sample concentration was measured with Qubit®/Quant-IT® Fluorometric
1078 Quantitation, Life Science Technologies. The library preparation was done according to the guidelines from
1079 Illumina Stranded mRNA Preparation, Illumina (1000000124518) using Illumina Stranded mRNA
1080 Preparation, Ligation, Kit (Illumina). The average fragment size was 335 bp. The base calling was done
1081 using the bcl2fastq2 software on NovaSeq 6000. Sequencing was done using Illumina NovaSeq 6000 S1
1082 v1.5, with paired-end sequencing and 2 x 50 bp read length.

1083 The read quality was checked with FastQC (v.0.11.8). The reads were aligned against the hg38 human
1084 genome (Illumina iGenome: https://support.illumina.com/sequencing/sequencing software/igenome.html
1085 (UCSC)) and annotated using the Rsubread package (v.2.6.4) in Bioconductor (v.3.13), R (v.4.1.0). The

gene ids were matched to the gene symbols using the org.Hs.eg.db package (v.3.13.0). Normalization was done with edgeR (v.3.34.1) to produce counts per million (CPM) and reads per kilo read per million (RPKM) for each gene. Pairwise comparisons between groups were performed using ROTS (v.1.20.0) on log2(1+CPM).

Western blot

All samples were lysed in 3x Laemmli buffer (0.1875 M Tris, 0.21 M SDS, 30% glycerol, bromphenol blue) containing 3% 2-mercaptoethanol (Merck, Cat. #444233) on ice, scraped into 1.5 ml centrifuge tubes, and boiled at 95°C for 10 minutes. The lysates were separated by SDS-PAGE and transferred onto nitrocellulose membranes (Cytiva, Cat. #15220033). The membranes were checked for loading using Revert™ 700 Total Protein Stain (LI-COR Cat. #926-11016), blocked with 1% w/v milk in PBS with 0.1% Tween 20 (VWR Cat. #M147) for 30 min and probed with the antibodies indicated below. The bands were visualized using SuperSignal™ West Picoplus chemiluminescent substrate kit (Thermo Fisher Scientific Cat. #34580) and imaged with iBright FL1000, Thermo Fisher Scientific. The bands were analyzed using the ImageStudio Lite software (v.6.0), LI-COR. Unless stated otherwise, all bands were normalized to total protein stain. The primary antibodies used: Notch2 1:1000 (Cell Signaling Cat. #5732), Notch3 1:1000 (Cell Signaling Cat. #5276), Jagged1 1:1000 (Cell Signaling Cat. #2620), α-SMA 1:1000(Cell Signaling Cat. #19245), Pdgfrβ 1:1000 (Cell Signaling Cat. #3169), β-tubulin 1:1000 (Cell Signaling Cat. #86298), His-Tag 1:1000 (Cell Signaling Cat. #2365), M2-Flag 1:1000 (Merck, Cat. #F1804), smad2/3 1:200 (Santa Cruz Cat. #sc-133098), and phospho-smad2 1:1000 (Cell Signaling Cat. #3108), β-actin 1:10000 (Merck Cat. #A1978). The horse radish peroxidase-conjugated secondary antibodies used: anti-rabbit 1:10000 (Vector Laboratories, #PI-1000), anti-mouse 1:10000 (Vector Laboratories, #PI-2000), Veriblot for IP detection 1:500 (Abcam, Cat. #ab131366).

Re-analysis of single-cell RNAseq data

For the vascular cells from different organs, previously published normalized datasets from the Betsholtz lab(2–4) were downloaded from Gene Expression Omnibus under the accession codes GSE98816 (brain), GSE20100 (lung), GSE210087 (heart), GSE210013 (colon), and GSE21000 (aorta). The expression matrices were read using the general Seurat scRNAseq analysis pipeline (v.4.4). For the datasets except the brain data, the ENSEMBL IDs were converted to gene symbols using Org.Mm.eg.db (v.3.20.0) and AnnotationDbi (v.1.68.0), and the duplicates and the entries without symbols were removed. Each dataset was then processed according to the Seurat workflow. Gene expression was normalized to 10000 counts and log-transformed. The clusters were created using the FindClusters function with the resolution set to 0.5 for the aorta dataset and 1 for the rest. The UMAP was calculated for brain, lung, heart, colon, and aorta datasets from the top 20, 25, 20, 20, and top 15 PCs, respectively. The cluster annotations were partly adapted from Muhl et al.(4). SMCs, Acta2, Myh11, Tagln, and Cspg4 were used as SMC markers, while Chrdl1, Hhip, Shisa3, Ccl19, Chrm2, Bdkrb2, and Abcc9 were used to filter out the non-arterial SMCs and pericytes. For the heart dataset, the cluster positive for Itgbl1 was annotated as aortic SMCs proximal to the heart. The clusters positive for Pecam1 and Kdr and negative for Prox1 were annotated as vascular endothelial cells. The clusters were extracted from the count matrices using the annotated cell IDs from the Seurat objects. The SMC and the EC data were processed separately. The datasets were filtered only to include the common genes among the different organs. The extracted matrices were re-normalized individually using “RC” transformation. No data integration or batch correction were deemed necessary as the datasets were used only for the comparison of single genes.

The processed mesoderm dataset was downloaded from Zebrahub. The expression matrix and the metadata files were extracted using the Scanpy tool in Python and used to create a Seurat object. This dataset was already log-normalized and scaled and did not contain the raw counts. Hence, the PCA analysis was done manually using the first 30 components. The clusters were found using the resolution

set to 0.2, and the UMAPs were found using the top 15 PCs. Datasets from different timepoints (batches) were integrated using harmony package. Markers for all clusters were found using the FindAllMarkers command. The markers for non-vascular associated SMC markers and cycling cells were checked using the Daniocell(5) single-cell RNAseq database. Based on this, the clusters highly expressing, desmb, nkx2.3, rem1, and tlx1 were used to filter out the non-vascular SMCs (Figure S4A). The remaining SMC clusters were annotated based on smooth muscle marker and notch3 expression. The VlnPlot function was used to plot the normalized counts based on the new annotations.

Computational Model for Extrinsic Ligand Induction

To simulate the experimental scenarios of Notch signaling in a cluster of SMCs, we extended a previous computational framework of Notch signaling (AB model developed by Loerakker et al.(6) and Ristori et al.(7), based on Sprinzak et al.(8) and Boareto et al.(9)) in a periodic one-dimensional array of SMCs, by incorporating the separate effects of Notch2-Jagged1 and Notch3-Jagged1 binding on the signaling dynamics. The levels of key proteins (Notch2, Notch3 Jagged, NICD) were predicted for each cell, with interactions allowed between neighboring cells on either side. The temporal changes in Notch (N), Jagged (J), and NICD (I) concentrations within cell i at time t were modeled using the following differential equations:

$$\frac{dN_3^i}{dt} = N_3^{pr} H\left(I_{N2}^i,\ I_{0,N2}, n_{N2}, \lambda_{N2}\right) H\left(I_{N3}^i,\ I_{0,N3}, n_{N3}, \lambda_{N3}\right) - N_3^i\left(k_c J^i + k_t J_{ext}^i\right) - \gamma N_3^i \quad (1)$$

$$\frac{dN_2^i}{dt} = N_2^{pr} - N_2^i\left(k_c J^i + k_t J_{ext}^i\right) - \gamma N_2^i \quad (2)$$

$$\frac{dJ^i}{dt} = J^{pr}\, H\left(I_{N2}^i,\ I_{0,J2}, n_{J2}, \lambda_{J2}\right) H\left(I_{N3}^i,\ I_{0,J3}, n_{J3}, \lambda_{J3}\right) - J^i\left(k_c N_3^i + k_t N_{3,\ ext}^i\right) - J^i\left(k_c N_2^i + k_t N_{2,\ ext}^i\right) - \gamma J^i$$
(3)

$$I_{N3}^i = k_t\, N_3^i\, J_{ext}^i - \gamma_I\, I_{N3}^i \quad (4)$$

$$I_{N2}^i = k_t\, N_2^i\, J_{ext}^i - \gamma_I\, I_{N2}^i \quad (5)$$

Here, N_2, N_3, J represent the Notch2, Notch3, and Jagged1 protein levels, and I_{N3}, I_{N3} represent the NICD content of the cell. $N_2^{pr}, N_3^{pr}, J^{pr}$ are the basal production rates of Notch2, Notch3 and Jagged1, respectively. k_c, k_t denote the cis-inhibition and trans-activation strength parameters, respectively. γ represents the degradation rate of Notch and Jagged and γ_I is the degradation rate of NICD. The effects of transactivation on the production rate of Notch3 and Jagged1 from NICD2 and NICD3 were incorporated with shifted Hill functions in the following form:

$$H^S(ICD, \lambda, n) = \lambda + \frac{1-\lambda}{1+\left(\frac{I}{I_0}\right)^n} \quad (6)$$

with I denoting the NICD content ($NICD_{N2}$ or $NICD_{N3}$) and λ defining the changes in protein production in response to Notch2/Notch3 transactivation. The parameter I_0 defines the transition point of the Hill function from convex to concave and the parameter n determines the sensitivity of protein production to the NICD content. A schematic illustration of the interactions in the model is shown in Figure S3B.

The initial values for the protein content of Notch2, Notch3, Jagged, and NICD for each cell were randomly generated between 0 and 6000 molecules, similar to Loerakker et al.(6) and Ristori et al.(7). The trans interactions occur with proteins located on the membranes of neighboring cells. Notch and Jagged were assumed to be distributed equally over the cell membrane, where half of the amount is available for binding with each of its neighbors. To replicate the experimental environment of a large number of closely packed

cells in a cluster, periodic boundary conditions were applied to the first and last cells in the simulated array. Hence the first cell was treated as a neighbor to the last cell, creating a continuous loop, thereby eliminating artificial edge effects that would otherwise arise if the array had distinct boundaries (Figure S3C). For all other cells, the external Notch and Jagged were defined in the following form:

$$N^{i}_{ext} = \frac{N^{i+1} + N^{i-1}}{2} \quad (7)$$

$$J^{i}_{ext} = \frac{J^{i+1} + J^{i-1}}{2} + J^{coat} \quad (8)$$

Where N^{i}_{ext} and J^{i}_{ext} represent the external Notch[2/3] and Jagged1 for cell i that is available to for Jagged-Notch signaling, respectively, and J^{coat} is the constant external Jagged coating.

In line with the experimental conditions, we simulated three different protein manipulation setups: (1) Control, with both Notch2 and Notch3 production; (2) siN2, with Notch2 production knocked down; and (3) siN3, with Notch3 production knocked down. These three scenarios were also tested with external Jagged1 coating, resulting in three additional setups: Control_J, siN2_J, and siN3_J, giving a total of six experimental scenarios. Each simulation was repeated 25 times, and all simulations reached a steady-state solution after a simulated time of 15 hours. The stable protein content values in the periodic model were found to be insensitive to the to the time increment when chosen ≤0.01 of the explicit time integration scheme and the number of cells when chosen ≥10 cells, hence a time increment of 0.01 and 10 cells were adopted. The final protein production levels were averaged across cells and repeated simulations for each experimental scenario.

Most of the parameter values regulating the dynamics of Jagged1–Notch2/3 signaling in SMCs were adopted from Boareto et al.(9). The basal production rates of Notch2 and Jagged1 were assumed to be half that of Notch3, which was set at 1000 h^{-1}, since based on RNAseq data, SMCs expressed 2-fold more copies of NOTCH3 than NOTCH2 at 24h (Figure S3 A). In addition, they seemed to express almost no other ligand than JAG1. The strengths of trans-activation (k_t) and cis-inhibition (k_c) were assumed 5×10^{-5} and 5×10^{-4}, respectively(6, 9). Hill function parameters were selectively optimized, with only the transition parameters $I0_{J3}$ and $I0_{N3}$ and sensitivity parameters n_{N2} and n_{N3} adopted from previous models(6, 9). The remaining parameters of the shifted Hill function were optimized to account for their potential influence on the results (see Table 1).

Table S1. Parameters of the shifted hill function characterizing the upregulation of Notch3 and Jagged 1 by NICD2 and NICD3 in the computational model.

Parameter	Description	Value/Range	Reference
λ_{N2}	Maximum fold change in **Notch** production rate from **Notch2**	To optimize [1,5]	
$I0_{N2}$	Transition parameter in **Notch** production rate from **Notch2**	To optimize [50,500]	
n_{N2}	Sensitivity parameter in **Notch** production rate from **Notch2**	2	(6, 8, 9)
λ_{N3}	Maximum fold change in **Notch** production rate from **Notch3**	To optimize [1.5,5]	(10)
$I0_{N3}$	Transition parameter in **Notch** production rate from **Notch3**	200	(6, 9)
n_{N3}	Sensitivity parameter in **Notch** production rate from **Notch3**	2	(6, 8, 9)

λ_{J2}	Maximum fold change in **Jagged** production rate from **Notch2**	To optimize [1,5]	
$I0_{J2}$	Transition parameter in **Jagged** production rate from **Notch2**	To optimize [50,500]	
n_{J2}	Sensitivity parameter in **Jagged** production rate from **Notch2**	To optimize [1,10]	
λ_{J3}	Maximum fold change in **Jagged** production rate from **Notch3**	To optimize [1.5,5]	(10)
$I0_{J3}$	Transition parameter in **Jagged** production rate from **Notch3**	200	(6, 9)
n_{J3}	Sensitivity parameter in **Jagged** production rate from **Notch3**	To optimize [1,10]	

We employed a Genetic Algorithm (GA) to optimize a set of eight parameters ($\lambda_{N2}, I0_{N2}, \lambda_{N3}, I0_{N3}, n_{N3}, \lambda_{J2}, I0_{J2}, n_{J2}, \lambda_{J3}, I0_{J3}, n_{J3}$) in the computational model of Notch signaling, aiming to minimize the Mean Squared Error (MSE) between simulated and experimental qPCR data at 24h from Figure 2 G for transmembrane proteins. The simulations were performed using MATLAB (The MathWorks Inc., v.R2025a). The objective function was defined to calculate the MSE between the normalized simulated outputs (averaged for cells at 24h) and the experimental data, using the Notch2-Notch3 signaling model. The GA was run with a maximum of 100 generations and the stopping criteria were set to three consecutive generations with no improvement, and a tolerance of 10^{-4}. The objective function calculated the Mean Squared Error (MSE) between simulated and experimental data for Notch2 (N2), Notch3 (N3) and Jagged1 (J1) relative expressions. As Notch2 is not influenced by Hill function parameters (Eq 2), the MSE was computed by summing the squared differences normalized values ($N_{3,j}^{sim}$ and J_j^{sim}) and ($N_{3,j}^{exp}$ and J_j^{exp}), where j denotes the index of the experimental scenario. Thus, the total MSE serves as the objective function (CF) that quantifies the difference between the two datasets.

$$N_{3,i}^{sim} = H\left(I_{N2}^{j}, I_{0,N2}, n_{N2}, \lambda_{N2}\right) H\left(I_{N3}^{j}, I_{0,N3}, n_{N3}, \lambda_{N3}\right) \quad (9)$$

$$J_j^{sim} = H\left(I_{N2}^{j}, I_{0,J2}, n_{J2}, \lambda_{J2}\right) H\left(I_{N3}^{j}, I_{0,J3}, n_{J3}, \lambda_{J3}\right) \quad (10)$$

$$MSE_{N3} = \sum_{i=1}^{6} (N_{3,i}^{sim} - N_{3,i}^{exp})^2 \quad (11)$$

$$MSE_J = \sum_{i=1}^{6} (J_i^{sim} - J_i^{exp})^2 \quad (12)$$

$$CF = MSE_{N3} + MSE_J \quad (13)$$

The optimization results including the best parameter values, number of iterations and the minimum cost value are given in Table 2.

Table S2. Optimized parameters of the Notch signaling model using the Genetic Algorithm under constraints of Table 1.

Optimized Parameters								**Iterations**	**Cost**
λ_{N2}	$I0_{N2}$	λ_{N3}	λ_{J2}	$I0_{J2}$	n_{J2}	λ_{J3}	n_{J3}		
2.57	50.24	1.56	4.52	76.38	1.89	1.82	1.76	65	0.68

The optimization results showed a stronger influence of NICD2 on transmembrane protein production (Notch and Jagged), compared to that of NICD3 ($\lambda_{J2}, \lambda_{N2} > \lambda_{J3}, \lambda_{N3}$). Additionally, $I0_{J2}, I0_{N2} < I0_{J3}, I0_{N3} =$

200 , which shows that NICD2 induces Notch and Jagged at lower thresholds than those of NICD3. To verify these findings, we repeated the optimization procedure with constraints that enforced the opposite conditions:

(1) NICD3 was set to have a stronger influence on the production of Jagged1 and Notch3 than NICD2 ($\lambda_{J3}, \lambda_{N3} > \lambda_{J2}, \lambda_{N2}$)
(2) NICD3 was assumed to induce Notch3 and Jagged1 production at lower thresholds than NICD2 ($I0_{J3}, I0_{N3} > I0_{J2}, I0_{N2}$)

The results of the verification run are shown in Table 3, where both constraints led to significantly higher minimum costs in the optimization algorithm, indicating that these alternative scenarios deviated from the experimental mean protein levels (see Table 3 and Figure S3G).

Table S3. Optimized parameters of the Notch signaling model after enforcing opposite conditions of the original results from Table 2.

Optimized parameters								Iterations	Cost
λ_{N2}	$I0_{N2}$	λ_{N3}	λ_{J2}	$I0_{J2}$	n_{J2}	λ_{J3}	n_{J3}		
Condition 1: $\lambda_{J3}, \lambda_{N3} > \lambda_{J2}, \lambda_{N2}$									
1.85	74.18	1.88	2.47	50.3	5.02	2.68	1.19	16	2.25
Condition 2: $I0_{J3}, I0_{N3} > I0_{J2}, I0_{N2}$									
4.56	415	1.93	2.56	484.1	1.90	3.26	4.89	14	10.92

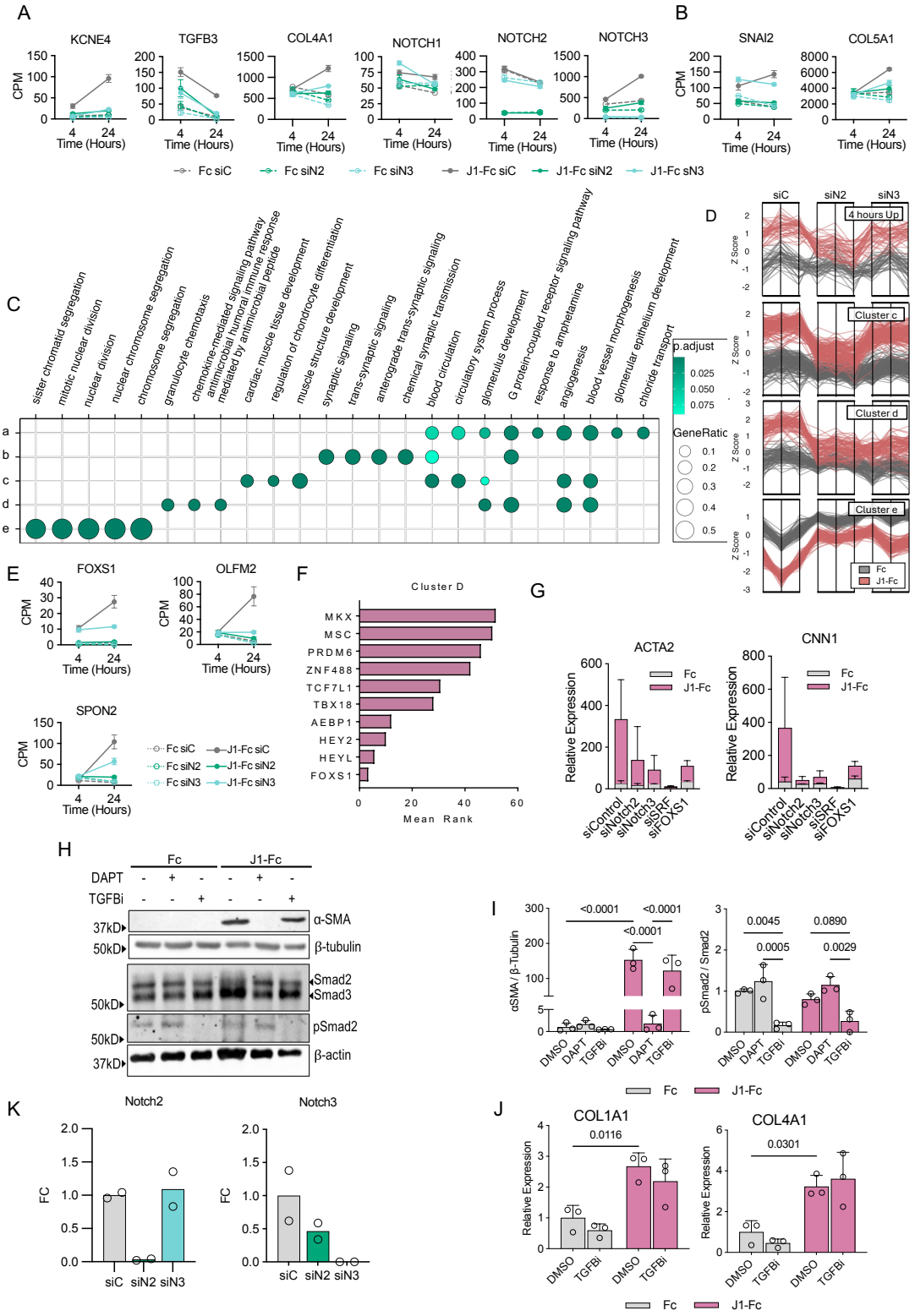
A
KCNE4
TGFB3
COL4A1
NOTCH1
NOTCH2
NOTCH3
CPM
Time (Hours)
Fc siC
Fc siN2
Fc siN3
J1-Fc siC
J1-Fc siN2
J1-Fc sN3
B
SNAI2
COL5A1
C
sister chromatid segregation
mitotic nuclear division
nuclear division
nuclear chromosome segregation
chromosome segregation
granulocyte chemotaxis
chemokine-mediated signaling pathway
antimicrobial humoral immune response mediated by antimicrobial peptide
cardiac muscle tissue development
regulation of chondrocyte differentiation
muscle structure development
synaptic signaling
trans-synaptic signaling
anterograde trans-synaptic signaling
chemical synaptic transmission
blood circulation
circulatory system process
glomerulus development
G protein-coupled receptor signaling pathway
response to amphetamine
angiogenesis
blood vessel morphogenesis
glomerular epithelium development
chloride transport
p.adjust
GeneRatio
D
siC
siN2
siN3
4 hours Up
Cluster c
Cluster d
Cluster e
Z Score
Fc
J1-Fc
E
FOXS1
OLFM2
SPON2
F
Cluster D
MKX
MSC
PRDM6
ZNF488
TCF7L1
TBX18
AEBP1
HEY2
HEYL
FOXS1
Mean Rank
G
ACTA2
CNN1
Relative Expression
siControl
siNotch2
siNotch3
siSRF
siFOXS1
H
Fc
J1-Fc
DAPT
TGFBi
α-SMA
β-tubulin
Smad2
Smad3
pSmad2
β-actin
37kD
50kD
I
αSMA / β-Tubulin
pSmad2 / Smad2
<0.0001
0.0045
0.0005
0.0890
0.0029
DMSO
DAPT
TGFBi
J
COL1A1
COL4A1
0.0116
0.0301
K
Notch2
Notch3
FC
siC
siN2
siN3

1243 **Fig. S1. Supplemental data relating to the bulk RNAseq and J1-induced gene expression.** (Related
1244 to Figure 1 and 2)
1245 (A, B) Selected genes from cluster d (A) and cluster c (B), regulated by Jagged1-Notch2/Notch3
1246 signaling. NOTCH1, NOTCH2, and NOTCH3 mRNA levels are given for reference.
1247 (C) Gene ontology analysis of the clusters from 24h as listed by the “clusterprofiler” package.
1248 (D) Behavior of the gene clusters upon different treatments: genes upregulated on immobilized J1-Fc at
1249 4h, 24h clusters c, d, and e, respectively.
1250 (E) Expression of FOXS1, OLFM2, and SPON2 based on RNAseq. FOXS1 was one of the top 10
1251 upregulated genes by J1-Fc stimuli at both time points (please see also Figure 1 C) (mean+SD, n=3
1252 independent experiments).
1253 (F) Genes from RNAseq cluster d were analyzed for transcription factor co-expression using the ChEA3
1254 web tool. The top 10 possible upstream transcription factors as listed by ChEA3 are listed with their mean
1255 rank (the lower the better) in the bar chart.
1256 (G) SMCs were treated with the indicated siRNAs for 48h and grown on immobilized J1-Fc for another
1257 48h. The indicated mRNAs were analyzed using qPCR, normalized to UBC, and presented as relative
1258 expression (mean+SD, n=2 independent experiments, one-way ANOVA followed by Dunnett´s test for
1259 multiple comparisons to the J1-Fc siControl. The comparisons of J1-Fc-treated samples with p values
1260 smaller than 0.1 are shown on the corresponding bars).
1261 (H-J) SMCs were grown on immobilized J1-Fc (72h for WB and 24h for qPCR) with 10μM DAPT, TGFβi,
1262 or DMSO and analyzed for the indicated molecules. The αSMA and phopho-Smad2 signals were
1263 normalized to β-tubulin, and total Smad2, respectively, and presented as fold change (I). For qPCR, the
1264 relative expression was normalized to UBC and presented as fold change (J) (mean+SD, n=3
1265 independent experiments, one-way ANOVA followed by Šídák's test for multiple comparisons. Pairwise
1266 comparisons with p values smaller than 0.1 are shown on the plots.).

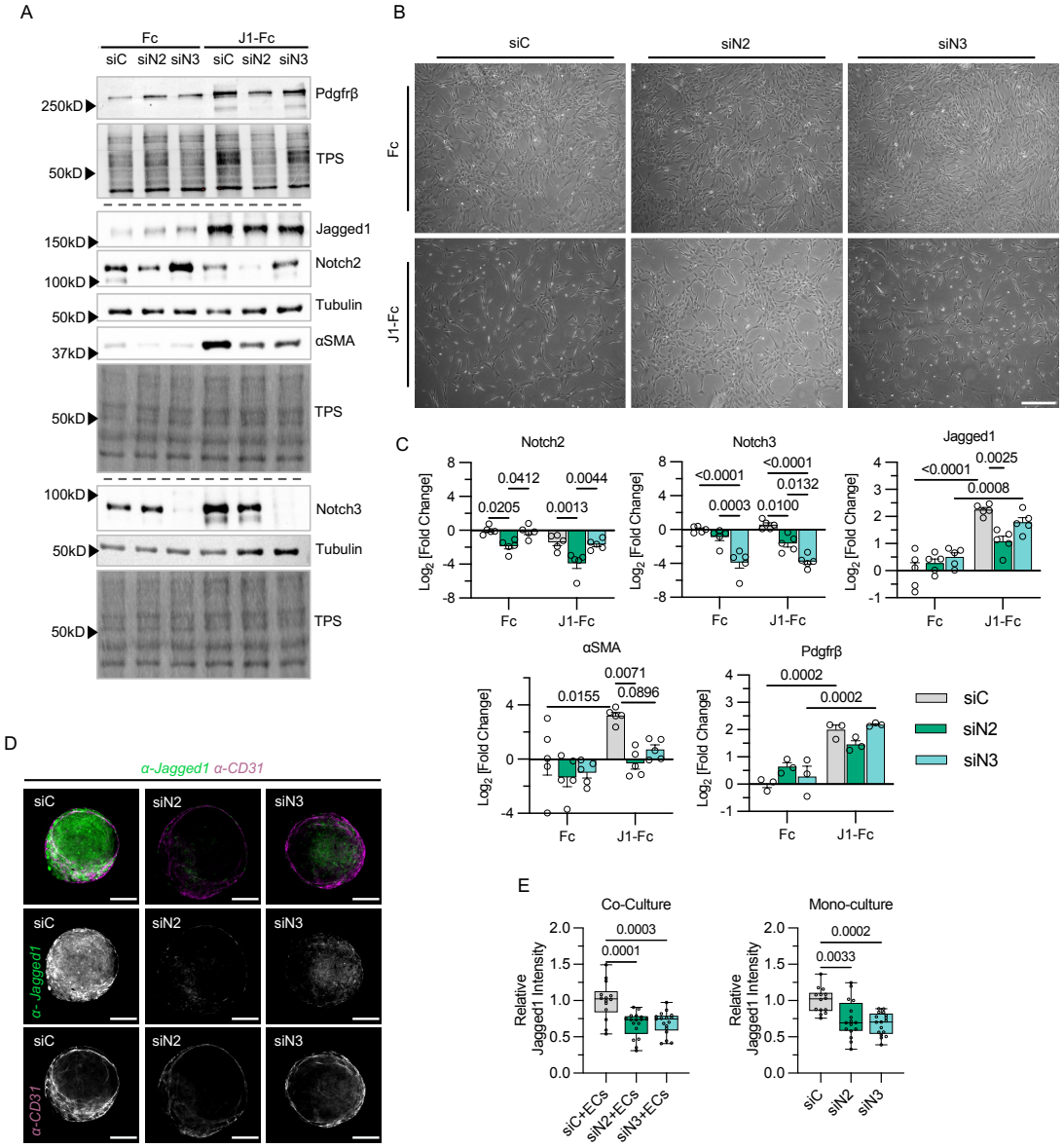

Fig. S2. SMC differentiation and Notch activation assays. (Related to Figure 1 and 2)
(A-C) SMCs were treated with the indicated siRNAs for 48h, then grown on immobilized J1-Fc for 72h and imaged (C) before immunoblotting for the indicated proteins(A). The signal was normalized to protein loading and presented as log2 fold change (B) (mean+SEM, n=5 (n=3 for Pdgfrβ) independent experiments, two-way ANOVA followed by Tukey´s test for multiple comparisons. Pairwise comparisons with p values lower than 0.1 are indicated on the plots).
(D, E) Notch2KD or Notch3KD SMCs were grown as spheroids in low-adhesion U-bottom plates for 72h (monoculture) or 48h before another 24h with human umbilical vein endothelial cells (co-culture). The spheroids were fixed and stained for Jagged1 or CD31. The representative confocal slices (D) and their mean Jagged1 intensity are shown (E) (Scale bars=150μm, error bars represent the min-max range, n=3

1278 independent experiments with at least 4 spheroids per condition, one-way ANOVA followed by Tukey´s
1279 test for multiple comparisons. Pairwise comparisons with p values lower than 0.1 are indicated on the
1280 plots.).
1281

1282

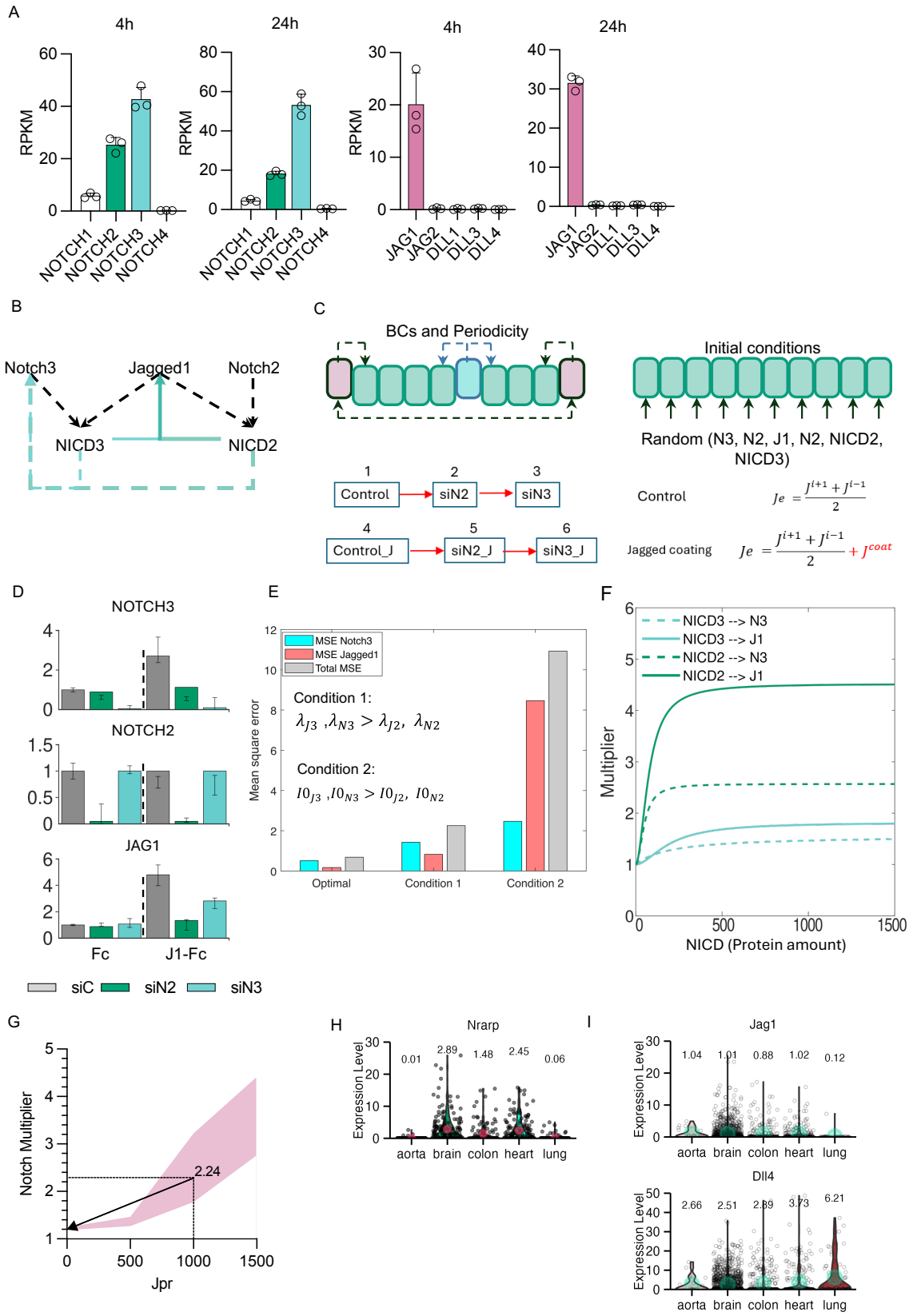
A
4h
24h
4h
24h
RPKM
NOTCH1
NOTCH2
NOTCH3
NOTCH4
JAG1
JAG2
DLL1
DLL3
DLL4
B
Notch3
Jagged1
Notch2
NICD3
NICD2
C
BCs and Periodicity
Initial conditions
Random (N3, N2, J1, N2, NICD2, NICD3)
Control
siN2
siN3
Control_J
siN2_J
siN3_J
Control
Jagged coating
D
NOTCH3
NOTCH2
JAG1
Fc
J1-Fc
siC
siN2
siN3
E
MSE Notch3
MSE Jagged1
Total MSE
Mean square error
Condition 1:
Condition 2:
Optimal
Condition 1
Condition 2
F
NICD3 --> N3
NICD3 --> J1
NICD2 --> N3
NICD2 --> J1
Multiplier
NICD (Protein amount)
G
Notch Multiplier
2.24
Jpr
H
Nrarp
Expression Level
aorta
brain
colon
heart
lung
I
Jag1
Dll4

1283 **Fig. S3. Supplemental data and illustrations relating to the computational model.** (Related to Figure
1284 3 and 4)
1285 (A) Basal expression of different Notch receptors and ligands in SMCs at 4h and 24h siC- and Fc-treated
1286 SMCs based on RNAseq (mean+SD).
1287 (B) Diagram depicting the causative relationship between Notch2, Notch3, and Jagged1 included in the
1288 theoretical framework used for building the computational model. Line weight denotes the strength of the
1289 interaction as informed by the experimental data from Figure 2.
1290 (C) Schematic one-dimensional array of vascular SMCs with periodic boundary conditions and initial
1291 random values of transmembrane and intracellular proteins (top). Experimental scenarios of protein
1292 manipulation with and without jagged coating with external jagged derivation for the cell (bottom).
1293 (D) Model validation was performed by enforcing assumptions (conditions 1 and 2) opposite to those the
1294 experimental data suggests (optimal). The simulated means against the experimental data (error bars)
1295 and the mean squared error for each condition are presented as bar plots.
1296 (E) Simulated results from the model showing the levels of the Notch signaling components in response
1297 to Jagged1 stimuli following parameter optimization. Bars and error bars represent simulated fold
1298 changes and the standard error in fold changes from the experimental data (24h) from Figure 2 G.
1299 (F) Hill curves resulting from the simulation with optimized parameters, showing the causative effect of
1300 Notch2 or Notch3 ICD on the production of Jagged1 and Notch3 as Notch signaling targets.
1301 (G) The predicted Notch signaling multiplier range in the aortic SMCs, was calculated using the ranges
1302 N2pr(428:642)(1/h) and N3Pr(857:1071)(1/h). Using N2Pr=500, N3Pr=1000, and Jpr=1000 produces a
1303 multiplier of 2.24. Jpr=0 reduces the multiplier to approximately 1.
1304 (H, I) Normalized expression of Notch target gene Nrarp in arterial SMCs (H) and Notch ligands Jag1 and
1305 Dll4 in vascular endothelial cells (I) of different mouse organs extracted from scRNAseq data (Muhl et al.;
1306 aorta, heart, colon, and lung) and (Vanlandewijck et al.; brain). The circles and the text above the violin
1307 plots denote the mean expression.
1308

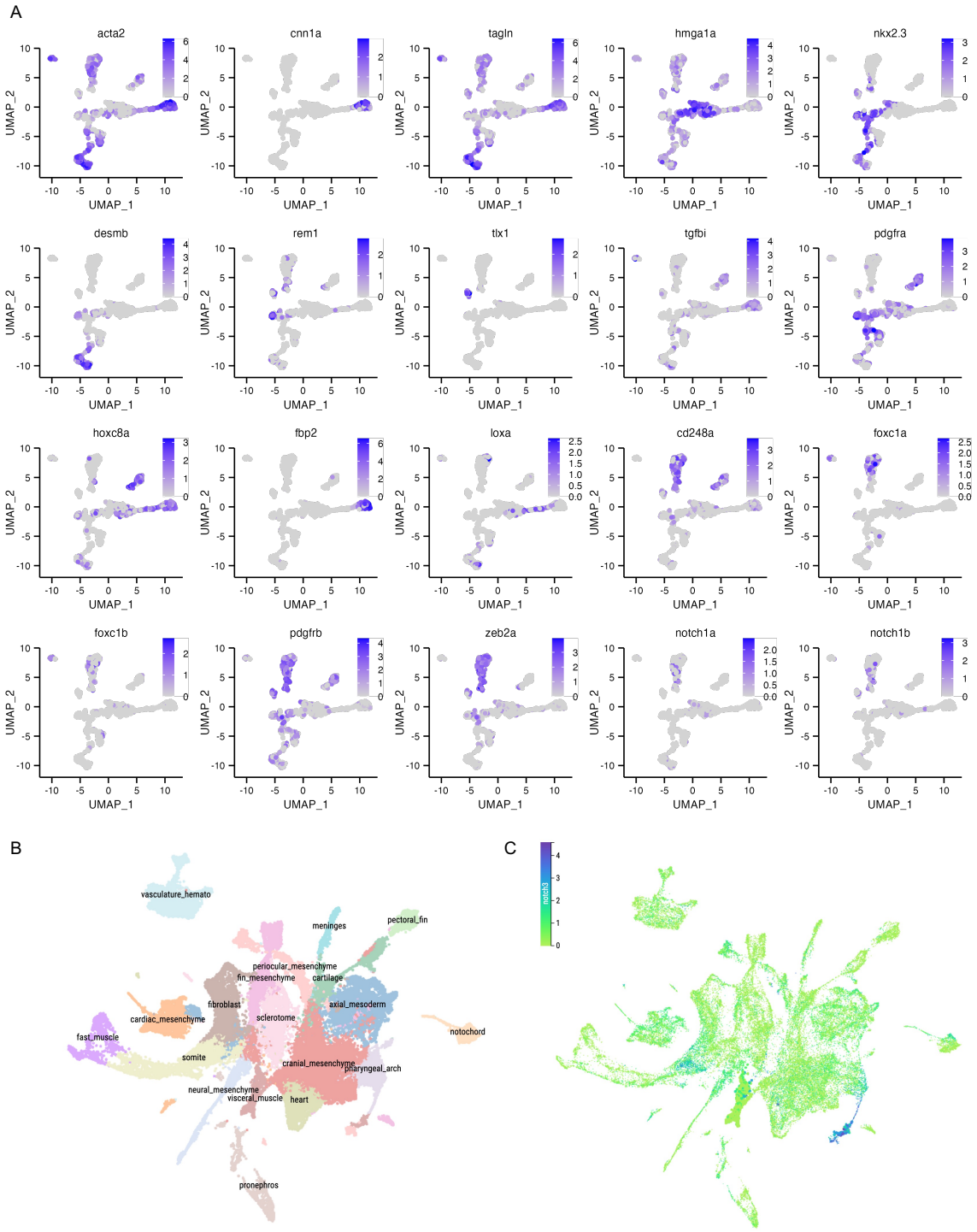

Fig. S4. Feature plots of selected genes related to Fig. 5 A-F and the clustering of the original mesoderm dataset from Zebrahub.

1312 *(A) Expression levels of smooth muscle markers (acta2, tagln, and cnn1a), cycling SMC marker hmga1a,*
1313 *visceral SMC markers (nkx2.3 and desmb), spleen SMC marker tlx1, fibroblast-like cell markers (tgfbi and*
1314 *pdgfra), positional markers (hoxc8a, hoxc1a, foxc1a-b, fbp2, loxa) and pericytic markers (cd248a, pdgfrb,*
1315 *zeb2a, and abcc9). (B, C) Expression of notch3 across Zebrahub mesoderm clusters – smooth muscle*
1316 *clusters indicated with larger dots.*

1317
1318

1319 **Table S4.** Reagents and other resources

REAGENT or RESOURCE	SOURCE	IDENTIFIER
BIOLOGICAL MODELS		
Human aortic smooth muscle cells	Lonza	Cat #CC2571 (Lot #0000369150 Age 43, Male)
Human aortic smooth muscle cells	Lonza	Cat #CC2571 (Lot #0000335663 Age 22, Male)
Human aortic smooth muscle cells	ATCC	Cat #PCS-100-012™ (Lot 80126171, Age 23, Female)
Human umbilical vein endothelial cells	Promocell	Cat #C-12200 (Lot info NA)
HEK 293T cells	NA	NA
Tg(tagln:GFP)	Turku Bioscience Zebrafish Core Facility	Ando et al.(11)
Tg(kdrl:mCherry)		Ando et al.(11)
Tg(UAS:EGFP, pdgfrb:GAL4FF)		NA
REAGENTS		
Dulbecco´s Modified Eagle´s Medium	Merck	Cat #D6429
Opti-MEM	Gibco	Cat #31985062
ReagentPack™ for subculturing	Lonza	Cat #CC50-34
Fetal Bovine Serum	Gibco	Cat #17914671
Goat Serum	Biowest	Cat #S2000
Bovine Serum Albumin	Merck	Cat #A9418
L-glutamine	Merck	Cat #G7513
Penicillin/Streptomycin	Merck	Cat #P0781
PBS	Biowest	Cat #L0616
Revert™ 700 Total Protein Stain	LI-COR	Cat # 926-11016
NucleoSpin RNA	Macharey-Nagel	Cat #740955

SensiFAST™ cDNA Synthesis Kit	Bioline	Cat #Bio-65054
RNAiMAX Lipofectamine®	Thermo Fisher Scientific	Cat #13778150
JetOTIMUS®	Sartorius	Cat #101000006
SB-431542	MedChem Express	Cat #HY-10431
DAPT ((2S)- N- [(3,5-Difluoro phenyl)acetyl]- L-alanyl- 2-phenyl]glycine 1,1-dimethyl ethyl ester)	Bio-Techne	Cat # 2634-10
RNAScope™ Protease Plus	Bio-Techne	Cat #322331
HCR™ Gold RNA	Molecular Instruments	NA
5x HOT FIREPol EvaGreen qPCR Mix Plus	Labnet	Cat #08-24-00001-10
Dimethyl sulfoxide	Merck	Cat #D2650
Vectashield	Vector Laboratories	Cat #H-1000
5x Passive Lysis Buffer	Promega	Cat #E1941
VivoGlo™ luciferin	Promega	Cat #P1041
Nuncleon™ Sphera™ low adhesion plates	Thermo Fisher Scientific	Cat #174929
Triton X-100	VWR	Cat #M143
Glycerol	Merck	Cat #G5516
2-mercaptoethanol	Merck	Cat #444233
Nitrocellulose membrane	Cytiva	Cat #15220033
Tween 20	VWR	Cat # M147
SuperSignal™ West Picoplus	Thermo Fisher Scientific	Cat # 34580
cOmplete™ protease inhibitor	Roche	Cat #05892970001

Anti-Flag affinity agarose beads	Merck	Cat #A2220
ANTIBODIES AND RECOMBINANT PROTEINS		
αSMA Rabbit mAb (WB 1:1000)	Cell Signaling Technology	Cat #19245 Clone: D4K9N
β-tubulin Mouse mAb (1:1000)	Cell Signaling Technology	Cat #86298 Clone:D3U1W
β-actin Mouse mAb (WB 1:10000)	Merck	Cat #a1978 Clone:AC-15
Notch2 Rabbit mAb (WB 1:1000)	Cell Signaling Technology	Cat #5732 Clone:D76A6
Notch3 Rabbit mAb (WB 1:1000)	Cell Signaling Technology	Cat #5276 Clone:D11B8
Jagged1 Rabbit mAb (WB 1:1000, ICC 1:100)	Cell Signaling Technology	Cat #2620 Clone:28H8
CD31 Mouse mAb ((ICC 1:100)	Thermo Fisher Scientific	Cat #37-0700 Clone:MEM-05
Pdgfrβ Rabbit mAb (WB 1:1000)	Cell Signaling Technology	Cat #3169 Clone: 2E81
Flag Mouse mAb (WB 1:1000)	Merck	Cat #F1804 Clone: M2
His Rabbit pAb (WB 1:1000)	Cell Signaling Technology	Cat #2365
Phospho Smad2 (Ser465/467) WB Rabbit mAb (WB 1:1000)	Cell Signaling Technology	Cat #3108 Clone:138D4
Smad2/3 (WB 1:200)	Santa Cruz Biotechnology	Cat #sc-133098 Clone:C-8
Anti-Rabbit Goat Ab (WB 1:10000)	Vector Laboratories	Cat #PI-1000
Anti-Mouse Horse Ab (WB 1:10000)	Vector Laboratories	Cat #PI-2000
Veriblot (WB:1:500)	Abcam	Cat #ab131366
Pierce Recombinant Protein G	Thermo Fisher Scientific	Cat #77675

Recombinant human Jagged1-Fc	Bio-techne	Cat #1277-JG
Recombinant human IgG Fc	Bio-Techne	Cat #110-HG
anti-human Alexa fluor 488 antibody	Thermo Fisher Scientific	Cat #21091
anti-rabbit Alexa fluor 488	Thermo Fisher Scientific	Cat #A-11034
anti-mouse Alexa fluor 555	Thermo Fisher Scientific	Cat #A-21422
OLIGONUCLEOTIDES, qPCR PRIMERS, AND PLASMIDS		
siMAX non-targeting control siRNA siControl	Eurofins Genomics	Sequence: 5'-CCU ACA UCC CGA UCG AUG AUG-3'
ON-TARGETplus Human NOTCH2 siRNA -SMARTpool	Horizon Discovery	Cat #L-011093-00-0005
ON-TARGETplus Human NOTCH3 siRNA -SMARTpool	Horizon Discovery	Cat #L-012235-00-0005
ON-TARGETplus Human FOXS1 siRNA -SMARTpool	Horizon Discovery	Cat #L-009029-00-0005
ON-TARGETplus Human SRF siRNA -SMARTpool	Horizon Discovery	Cat #L-009800-00-0005
HCR™ *in situ* hybdridization chain reaction probe for *D. rerio* notch2-x2	Molecular Instruments	NA
HCR™ *in situ* hybdridization chain reaction probe for *D. rerio* notch3-x1	Molecular Instruments	NA
12xCSL-Luciferase	Kato et al. 1997 (https://doi.org/10.1242/dev.124.20.4133)	NA
p3xFlag-CMV		NA

p3xFlag Notch1 ICD CMV	Santio et al., 2016 (https://doi.org/10.18632/oncotarget.9215)	NA
p3xFlag Notch2 ICD CMV		NA
p3xFlag Notch3 ICD CMV		NA
p6xHis-3xGS-RBPJκ CMV	This paper	VectorBuilder ID: VB221019-1188trx
ACTA2, human	TAG Copenhagen	Forward: CGTGTTGCCCCTGAAGAGCAT, Reverse: ACCGCCTGGATAGCCACATACA
HEY1, human	TAG Copenhagen	Forward: TGGATCACCTGAAAATGCTG, Reverse: CGAAATCCCAAACTCCGATA
JAG1, human	TAG Copenhagen	Forward: AATGGCTACCGGTGTGTCTG, Reverse: CCCATGGTGATGCAAGGTCT
NOTCH2, human	TAG Copenhagen	Foward: AAGGAACCTGCTTTGATGACA, Reverse: CAGGGAGCCAATACTGTCTGA
NOTCH3, human	TAG Copenhagen	Forward: CCTAGTCCTGGCTCCGAAC, Reverse: GAGCCGGTTGTCAATCTCC
UBC, human	TAG Copenhagen	Forward: CAC TTG GTC CTG CGC TTG A, Reverse: CAATTGGGAATGCAACAACTTTAT
COL1A1, human	TAG Copenhagen	Forward: GCCAAGACGAAGACATCCCA Reverse: GGCAGTTCTTGGTCTCGTCA
COL4A1, human	TAG Copenhagen	Forward: ACCTGGATTTCAGGGGATGC Reverse: CGGCCTATGAGTCCTGGGTA
Notch2 morpholino	Gene Tools	NA

Notch3 morpholino	Gene Tools	NA
Control morpolino	Gene Tools	NA
SOFTWARE		
Matlab	Mathworks	v.2025a
Image Studio Lite	LI-COR	v.6.0
Prism	Graphpad	v.10
FlowJo	BD Biosciences	v.10
R	NA	v.4.1.0
Seurat	Satija Lab	v.4.4.0
Arivis Vision 4D	Zeiss	v.3.5.0
Imaris	Oxford Instruments	v.10.2.0
Fiji ImageJ	NA	v.2.16.0

Dataset S1 (Supplemental_Data_Table_S1.xlsx). Differentially expressed genes in non-targeting control siRNA-transfected SMCs upon J1-Fc induction and their clustering.

SI References

1. C. Sahlgren, M. V. Gustafsson, S. Jin, L. Poellinger, U. Lendahl, Notch signaling mediates hypoxia-induced tumor cell migration and invasion. *Proceedings of the National Academy of Sciences* **105**, 6392–6397 (2008).

2. L. He, *et al.*, Single-cell RNA sequencing of mouse brain and lung vascular and vessel-associated cell types. *Sci Data* **5**, 180160 (2018).

3. M. Vanlandewijck, *et al.*, A molecular atlas of cell types and zonation in the brain vasculature. *Nature* **554**, 475–480 (2018).

4. L. Muhl, *et al.*, A single-cell transcriptomic inventory of murine smooth muscle cells. *Dev Cell* **57**, 2426-2443.e6 (2022).

5. A. Sur, *et al.*, Single-cell analysis of shared signatures and transcriptional diversity during zebrafish development. *Developmental Cell* **58**, 3028-3047.e12 (2023).

6. S. Loerakker, *et al.*, Mechanosensitivity of Jagged–Notch signaling can induce a switch-type behavior in vascular homeostasis. *Proceedings of the National Academy of Sciences* **115**, E3682–E3691 (2018).

7. T. Ristori, O. M. J. A. Stassen, C. M. Sahlgren, S. Loerakker, Lateral induction limits the impact of cell connectivity on Notch signaling in arterial walls. *International Journal for Numerical Methods in Biomedical Engineering* **36**, e3323 (2020).

8. D. Sprinzak, *et al.*, Cis-interactions between Notch and Delta generate mutually exclusive signalling states. *Nature* **465**, 86–90 (2010).

9. M. Boareto, *et al.*, Jagged–Delta asymmetry in Notch signaling can give rise to a Sender/Receiver hybrid phenotype. *Proc. Natl. Acad. Sci. U.S.A.* **112** (2015).

10. H. Liu, S. Kennard, B. Lilly, NOTCH3 Expression Is Induced in Mural Cells Through an Autoregulatory Loop That Requires Endothelial-Expressed JAGGED1. *Circulation Research* **104**, 466–475 (2009).

11. K. Ando, *et al.*, Clarification of mural cell coverage of vascular endothelial cells by live imaging of zebrafish. *Development* **143**, 1328–1339 (2016).